

 Open access • Posted Content • DOI:10.1101/2020.05.25.115287

Single cell analysis of human site-specific melanocyte differentiation and the decoding of developmental programs in melanoma — [Source link](#)

Rachel L. Belote, Daniel D. Le, Ashley Maynard, Ursula E. Lang ...+7 more authors

Institutions: Huntsman Cancer Institute, University of California, Berkeley, University of Utah

Published on: 28 May 2020 - bioRxiv (Cold Spring Harbor Laboratory)

Topics: Melanocyte differentiation

Related papers:

- [Human melanocyte development and melanoma dedifferentiation at single cell resolution](#)
- [Developmental pathways activated in melanocytes and melanoma.](#)
- [New perspectives on melanoma: The role of PAX3](#)
- [Expression signatures of early-stage and advanced medaka melanomas.](#)
- [The neoplastic development of malignant melanoma. A biological rationale.](#)

Share this paper:    

View more about this paper here: <https://typeset.io/papers/single-cell-analysis-of-human-site-specific-melanocyte-3huv07og95>

Human melanocyte development and melanoma dedifferentiation at single cell resolution.

Rachel L. Belote^{1*}, Daniel Le^{2*}, Ashley Maynard³, Ursula E. Lang⁴, Adriane Sinclair⁵, Vicente Planells-Palop⁶, Laurence Baskin⁶, Aaron D. Tward⁶, Spyros Darmanis^{2†} and Robert L. Judson-Torres^{1,7,†,‡}

⁽¹⁾ Huntsman Cancer Institute, University of Utah, Salt Lake City, UT, USA

⁽²⁾ Department of Microchemistry, Proteomics, Lipidomics and Next Generation Sequencing, Genentech, Inc., South San Francisco, CA, USA.

⁽³⁾ Chan Zuckerberg Biohub, San Francisco, CA, USA

⁽⁴⁾ Department of Dermatology and Department of Pathology, University of California, San Francisco, CA, USA

⁽⁵⁾ Department of Urology and Division of Pediatric Urology, University of California, San Francisco, CA, USA

⁽⁶⁾ Department of Otolaryngology–Head and Neck Surgery, University of California, San Francisco, CA, USA

⁽⁷⁾ Department of Dermatology, University of Utah, Salt Lake City, UT, USA

Author list footnotes:

*These authors contributed equally

† Correspondence: darmanis@gene.com, judsontorreslab@gmail.com

‡ Lead contact

SUMMARY:

In humans, epidermal melanocytes are responsible for skin pigmentation, defense against ultraviolet radiation, and the deadliest common skin cancer, melanoma. While there is substantial overlap in melanocyte development pathways between different model organisms, species dependent differences are frequent and the conservation of these processes in human skin remains unresolved^{1–3}. Thus, the biology of developing and adult human melanocytes remains largely uncharacterized. Here, we used a single-cell enrichment and RNA-sequencing pipeline to study human epidermal melanocytes derived directly from skin, capturing transcriptomes across different anatomic sites, developmental age, sexes, and multiple skin tones. Using donor-matched skin from distinct volar and non-volar anatomic locations, we uncovered subpopulations of melanocytes exhibiting site-specific enrichment that occurs during gestation and persists through adulthood. In addition, we identified human melanocyte differentiation transcriptional programs that are distinct from gene signatures generated from model systems. Finally, we use these programs to define patterns of dedifferentiation that are predictive of melanoma prognosis. Overall, the characterization of human melanocytes fresh from skin revealed new subpopulations, human-specific transcriptional programs, and valuable insights into melanoma dedifferentiation.

INTRODUCTION:

Epidermal melanocytes, the pigment producing cells of human skin, are responsible for skin tone and orchestrate the primary defense against damage from ultraviolet (UV) radiation. Some anatomic site-specific differences in pigmentation are due to environmental factors, such as the tanning response to UV exposure. Others, like the hypopigmentation at volar sites (such as palms and soles), are present at birth. In adult skin, mesenchymal – epithelial interactions are known to influence anatomic site-specific melanocyte survival and pigment production⁴ but melanocyte intrinsic factors that contribute to site-specific specialization remain unclear.

Model organisms are powerful tools for investigating melanocyte development. In chick and mouse, a transient, multipotent neural crest cell population gives rise to committed immature melanocyte precursors, called melanoblasts, via two spatially and temporally distinct pathways^{2,3}. Such studies focus primarily on melanocytes in skin appendages (hair follicle, feather, and sweat gland). However, despite constituting the predominate subtype in human skin, resident epidermal melanocytes have not been the subject of analogous investigations into developmental trajectories and anatomic-specializations.

Melanocytes can give rise to melanomas which present distinct phenotypic and genomic characteristics correlated with primary tumor location^{5,6}. Like many cancers, melanoma progression is coupled to dedifferentiation of the cell of origin⁷. The aggressive nature of melanoma is proposed to be rooted in unique attributes of the melanocytic lineage⁸. Decoding the transcriptome of epidermal melanocytes across the human body during

53 development and in aged skin would provide further insight into the precise origins of melanoma and the
54 developmental programs reacquired during progression.

55

56 **Multi-site scRNA-seq of normal human melanocytes**

57 We performed single cell RNA sequencing (scRNA-seq) on 34 healthy skin specimens across multiple
58 anatomic locations (leg, arm, foreskin, palm and sole) from 22 donors aged 9.5 fetal weeks (f.w.) to 81 years (Fig.
59 1a, Supplementary Table 1) representing multiple skin tones and sexes. For each specimen, the epidermis was
60 enzymatically removed from the dermis and dissociated into a single cell suspension. Since melanocytes comprise
61 a small fraction of the total epidermal cell mass, FACS was used to increase the capture rate of CKIT+ melanocytes
62 within the basal layer⁹⁻¹¹ (Fig. 1a, Extended Data Fig. 1a,b, and methods). Sorted cells were then processed using
63 the Smartseq2 single-cell RNA-seq protocol¹². After quality control (Extended Data Fig. 1c-e, methods) and iterative
64 Louvain clustering (see methods), differential expression was used to annotate 9,719 cells into the following cell-
65 types: melanocytes, keratinocytes, eccrine sweat gland cells, and three immune cell populations (Fig. 1b,c and
66 Extended Data Fig. 1f-i). Individual cells were then designated as cycling or non-cycling based on expression of
67 established marker genes (Extended Data Fig. 2a-c)¹³. To further investigate heterogeneity within melanocytes, we
68 performed Louvain clustering on melanocytes alone. The resulting 10 clusters did not correspond with skin tone,
69 sex, or donor. Based on the expression of the top 5 differentially expressed genes (DEGs) for each cluster, clusters
70 were binned into four groups (Extended Data Fig. 3a-d). These groupings corresponded with developmental age
71 (adult, neonatal, and fetal) as well as a small group of fetal melanocytes expressing established melanocyte stem
72 cell genes (Fig. 1d and Extended Data Fig. 3f,g). Interestingly, evaluation of donor skin anatomic location presented
73 volar vs non-volar sites as a possible source of heterogeneity within the adult and fetal groups (Fig. 1e).

74

75 **Anatomic site-enriched melanocyte sub-populations**

76 The anatomical location of skin influences melanocyte survival and function but it remains unclear how site-
77 specific specialization arises during melanocyte maturation⁴. UMAP segregation by anatomic location within the
78 adult and fetal groups suggested melanocytes exhibit site-specific transcriptomic differences that arise early during
79 development (Fig. 1e-f). To test this hypothesis, we queried donor matched volar and non-volar cutaneous
80 specimens that spanned 10 f.w. to 77 years, different sexes, and different skin tones for transcriptional programs
81 that distinguished volar vs non-volar cutaneous melanocytes across developmental ages (n=6 donors, n=17 skin
82 specimens, Fig. 2a and Supplementary Table 1,*). Differential gene expression analysis (Mann-Whitney U test,
83 Benjamini-Hochberg FDR < 5%) revealed 2,042 transcripts with site-specific expression in both fetal and adult
84 donors (Fig. 2b-c, Supplementary Table 2). Using binary expression of the top 10 volar and non-volar cutaneous
85 genes (see methods), we classified individual cells from the full cohort (n=22 donors, n= 34 skin specimens) as volar-
86 like (v-mel) and non-volar cutaneous-like (c-mel). While v-mels and c-mels were present in all anatomic locations in
87 both adult and fetal skin (Fig. 1d), v-mels were enriched in volar skin (mean: 94% ± 5% s.d. volar sites, ~7% ± 5 %
88 non-volar sites) and c-mels were enriched in non-volar cutaneous skin (mean: ~89% ± 9% non-volar sites, 5% ± 5%
89 volar sites). The presence of melanocytes with a c-mel signature in volar sites and melanocytes with the v-mel
90 signature in cutaneous sites indicated: 1) two distinct sub-populations of epidermal melanocytes exist in human
91 skin with anatomic site-specific enrichment, and 2) enrichment occurs during and persists after skin development.
92 This discovery was validated via RNA FISH and immunofluorescence using the v-mel and c-mel signature genes that
93 presented a striking level of inverse expression between volar and non-volar cutaneous melanocytes across all
94 donor-matched skin: *NTRK2* (neurotrophic receptor tyrosine kinase 2) and *HPGD* (15-hydroxyprostaglandin
95 dehydrogenase), respectively (Fig. 2e-h, Extended Data Fig. 4). These observations further suggest the previously
96 reported site specific mesenchymal-melanocyte interactions^{4,14} that drive the epidermal phenotype in fully-
97 developed skin, provide more permissive, but non-exclusive, conditions for one melanocyte subpopulation over
98 another.

99

100 **Human-specific melanocyte differentiation programs**

101 We captured three broad developmental ages in our cohort: fetal, neonatal, and adult. Consistent with the
102 age based UMAP cluster arrangement, both diffusion pseudotime analysis and pairwise differential gene expression
103 showed a progression from fetal to adult with neonatal melanocytes as an intermediate transcriptional state
104 (Extended Data Fig. 5 and Supplementary Table 3). Our analyses did not reveal significant further transcriptional
105 changes associated with donor age in adult melanocytes.

106 To identify gene signatures that best distinguished each human melanocyte developmental group, a
107 regularized logistic regression model was trained using the single cell transcriptomes from 66% of the dataset
108 representing the four developmental stages (Fig. 3a). The resultant Developmental stage Melanocyte (DevMel)
109 model demonstrated excellent classification accuracy when tested on the holdout set, with f1-scores ranging from
110 0.93-1.00 (Extended Data Fig. 6a). Elastic net regularization yielded genes that collectively constituted
111 developmental stage-specific expression programs: prg[MSC], prg[FET], prg[NEO] and prg[ADT] (Fig. 3b, Extended
112 Data Fig. 6b-e and Supplementary Table 4).

113 To benchmark human melanocyte development against known mammalian developmental systems, we
114 assessed the expression of gene signatures previously defined during mouse melanocyte development¹⁵⁻¹⁸ and *in*
115 *vitro* differentiation of human ES cells into mature melanocytes¹⁹ within adult (ADT), neonatal (NEO), fetal (FET) and
116 melanocyte stem cells (MSCs) from c-mel enriched (non-volar cutaneous) skin (Extended Data Fig. 7 and
117 Supplemental Discussion). Mouse melanocyte cell-type-specific signatures were more highly expressed in FET, NEO,
118 and ADT melanocytes compared to MSC (p-value < 1e-12, Extended Data Fig. 7b,d). Alternatively, the mouse E14.5
119 and E17.5 melanoblast-specific signature¹⁶ was most highly expressed in MSC (> 1.5 fold change when compared to
120 each other group, p-value < 1e-7, Extended Data Fig. 7c), suggesting the MSC cluster is associated with hair follicle
121 development (see Supplemental Discussion). Consistent with this finding, the CD34+ mouse hair follicle melanocyte
122 stem cell gene set²⁰ was most highly expressed in MSC (p-value = 5.4e-38, Extended Data Fig. 7e). Of the *in vitro*
123 differentiation programs, the mature differentiated melanocyte program was expressed across all developmental
124 groups with the highest expression in FET, NEO and ADT groups compared to MSC (p-value < 1e-14, Extended Data
125 Fig. 7f).

126 Comparison of DevMel programs to those identified in mouse or in human *in vitro* differentiation yielded
127 sparse overlap (Extended Data Fig. 7g-j), indicating that our approach revealed previously unidentified programs
128 specific to human fetal, neonatal, and adult skin. We therefore sought to determine whether profiles unique to
129 human *in vivo* development could provide insight into melanoma dedifferentiation and aggression.

130

131 **Heterogenous reacquisition of developmental programs during tumorigenesis**

132 Melanoma progression often coincides with the loss of melanocyte differentiation markers and
133 upregulation of genes associated with earlier stages of development^{16,20-23}. This process is broadly described as
134 dedifferentiation. Given the known substantial cell-to-cell intratumor heterogeneity of melanoma²⁴, we reasoned
135 that single cells within a tumor might occupy various stages of dedifferentiation and that the proportion of cells in
136 each state potentially influences overall patient outcome. To assess tumor heterogeneity as captured by the
137 expression of human development-associated programs, we classified published single-cell malignant melanoma
138 samples^{25,26} using our DevMel model (Fig. 3c). We observed inter- and intra-tumor heterogeneity in the
139 representation of each melanoma group (Fig. 3d), indicating tumors are composed of a mix of dedifferentiated
140 states in line with our initial hypothesis. Similar to our analysis of model system developmental programs, the
141 MAL^{MSC} melanoma cells corresponded with stem cell-like transcriptional states (invasive, MITF-low, slow cycling)
142 previously identified in human melanomas (Extended Data Fig. 8b-e, see Supplemental Discussion). In addition, we
143 observed little developmental group specific enrichment for other reported melanoma signatures amongst the
144 other MAL groups (Extended Data Fig. 8d). Taken together, these data showed classification of melanoma cells by
145 human developmental programs generated a unique subdivision of non-stem like states, which could perhaps offer
146 further insight toward understanding other states of differentiation in melanoma.

147 To better define the course of dedifferentiation during melanoma progression, we looked for differential
148 gene expression patterns across each of the four MAL groups that were consistent with different forms of cellular
149 reprogramming: (1) a retrograde unfolding of the differentiation cascade (sequential dedifferentiation)²⁰, (2) direct
150 reprogramming to a more pluripotent stage (direct dedifferentiation), or (3) the acquisition of a melanoma-specific
151 program (Fig. 3b). Of 511 total unique genes, inclusive of DevMel model variables and MAL group top differentially
152 expressed genes (Extended Data Fig. 8a, Supplementary Table 5), 45% exhibited expression patterns consistent with
153 sequential dedifferentiation, in which the relative expression across healthy melanocyte developmental groups was
154 conserved among MAL groups (Fig. 3d). We found that 3.1% of genes exhibited a direct dedifferentiation pattern,
155 indicating that expression of these genes may be a prerequisite for disease progression and metastasis (Fig. 3e).
156 Supporting this interpretation, the small set of genes includes known markers of aggressive melanoma such as AXL
157 and HMGA2^{26,27}. Similarly, recently identified therapeutic resistance programs were evident in both the MSC
158 healthy and MAL^{MSC} populations (Extended Data Figure 8e). We also identified genes expressed in healthy

159 melanocyte groups that were down regulated in all melanoma groups (Fig. 3f), thus characterizing aspects of normal
160 melanocyte expression that are either non-essential or potentially inhibitory to melanoma progression and/or
161 metastasis.

162 Finally, 52 highly expressed genes in melanoma were absent from each of the healthy melanocyte
163 developmental groups (Fig. 3g and Supplementary Table 5). Among the top differentially expressed genes was the
164 melanoma-associated antigen PRAME, further supporting its use as a melanoma molecular diagnostic. Other of
165 these “melanoma specific” genes might be important for melanoma progression or diagnosis such as the MTRNR2L
166 family of transcripts, which encode for short peptides with anti-apoptotic activity²⁸, and were highly and exclusively
167 expressed in all melanoma groups.

168 169 **Developmental stage programs predict patient survival**

170 To determine whether gene expression programs characteristic of different human developmental ages
171 offer prognostic value, we applied CIBERSORT²⁹ to estimate the fraction of melanoma cells similar to ADT, NEO, FET,
172 MSC for all skin cutaneous melanoma (SKCM) tumor samples from The Cancer Genome Atlas (TCGA)³⁰. Similar to
173 the single cell melanoma dataset (Fig. 3d), we observed inter-tumor heterogeneity in the fractional representation
174 of the four developmental groups (Fig. 4a). Hierarchical clustering of SKCM label distributions classified tumor
175 samples according to the observed predominant developmental group: SKCM^{ADT}, SKCM^{NEO}, SKCM^{FET}, SKCM^{MSC}
176 (Supplementary Table 6). Neither genetic driver nor tumor site correlated with the developmental group
177 classification of the tumor (Fig 4a; Extended Data Fig. 8f).

178 Using our developmentally-defined subclasses of melanoma tumors, we evaluated the correlation of bulk
179 tumor differentiation status with patient outcome. As expected, the most differentiated group (SKCM^{ADT}) exhibited
180 best median overall survival (SKCM^{ADT} = 11.0 yr vs rest = 5.3 yr). Surprisingly, the most dedifferentiated groups
181 (SKCM^{FET}, SKCM^{MSC}) were not associated with worse outcomes (Fig. 4b); rather, the intermediately differentiated
182 group (SKCM^{NEO}) exhibited the shortest median overall survival (SKCM^{NEO} = 4.2 yr vs rest = 8.2 yr). To better
183 understand this unexpected finding, we evaluated the expression of transcriptional programs associated with
184 clinical response to therapeutics. Indeed, SKCM^{NEO} tumors expressed higher levels of transcripts associated with
185 immune resistance²⁵ (p-value=1.6e-2, SKCM^{NEO} vs rest) and a dearth in immune infiltration signatures²⁵(p-
186 value=5.5e-4, SKCM^{NEO} vs rest) as well as FDA-approved therapeutic targets³¹ (p-value=1.6e-5, SKCM^{NEO} vs rest)
187 (Extended Data Fig. 8g). The SKCM^{MSC} tumor group was unique in its increased expression of FDA-approved
188 therapeutic targets (p-value=4.6e-21, SKCM^{MSC} vs rest). These data are in agreement with previous studies^{20,25} and
189 demonstrate that while some amount of dedifferentiation is associated with worse prognosis, overall survival,
190 immune evasion and immune resistance are not linearly correlated with dedifferentiation (Fig. 4c). Taken together,
191 classification using human epidermal melanocyte developmental stage signatures revealed that at least four states
192 of dedifferentiation constitute individual tumors, and that the proportion of melanocytes that have readopted a
193 neonatal-like signature is associated with worse prognosis (Fig. 4c-d). The NEO program is not enriched for any
194 previously identified melanoma transcriptional signature, suggesting its potential as prognostic biomarker remains
195 untapped (Fig. 4d and Extended Data Fig. 8).

196 197 **DISCUSSION:**

198 We have provided a fresh-from-skin human epidermal melanocyte dataset that is, to our knowledge, the
199 first human cell atlas entry that encompasses human development, sex and diverse race/ethnicities and includes
200 multiple donor-matched anatomic locations.

201 We identified a novel population of epidermal melanocytes that appear early during human development.
202 As the predominant class of melanocytes in volar regions, we speculate these v-mels could represent a distinct cell
203 of origin of acral melanomas - a subtype of melanoma defined by its presentation in these regions and associated
204 with distinct mutational landscapes and poor therapeutic response and overall survival^{32,33}. It is possible epidermal
205 v-mels are hypopigmented descendants of previously defined sweat gland stem cells³⁴ and/or v-mels and c-mels
206 are derived from the two known distinct lineage specification pathways². Here we have provided markers that
207 permit exploration of these hypotheses in future studies.

208 By characterizing melanoma dedifferentiation using human-specific developmental programs, our work
209 sheds new light on the relationships among developmental stages, tumor characteristics, and melanoma cell
210 transcriptional states (Fig. 4c,d). For example, with 63 years as the average age of melanoma diagnosis, our *in situ*
211 adult melanocyte transcriptome provides a relevant basis for interrogating disease etiology and progression³⁵.

212 Moreover, our analyses identified the transcriptional state associated with neonatal melanocytes correlated to
213 worst overall survival. Due to tissue availability and ease of culture, the neonatal melanocyte transcriptome is often
214 considered the baseline “normal differentiated program” for comparison to melanoma transcriptomes. This
215 technical artifact can explain why this program has been previously underappreciated. We further identified
216 melanoma-specific genes directly acquired in all stages of dedifferentiation (Fig. 3f and Fig. 4d), suggesting that
217 these genes may undergo positive selection during early metastatic dissemination. Along with the widely-accepted
218 diagnostic melanoma biomarker PRAME³⁶ and an established marker of invasion AXL²⁶, we identified novel
219 melanoma-associated genes. Further investigation into the mechanistic roles of these gene sets could reveal novel
220 drivers of melanoma metastasis.

221 The findings presented here deliver a unique perspective on human melanocyte biology through the
222 characterization of distinct transcriptional programs specific to development and function. Thus, the transcriptional
223 programs identified here are valuable for understanding the diversity and malignant transformation of human
224 melanocytes.

225
226

227 **ACKNOWLEDGMENTS:**

228 We thank the University of California, San Francisco Biospecimen Resource Program for their help with tissue
229 acquisition, and Life Science Editors for critical editing of the manuscript. We thank the UCSF Program for
230 Breakthrough Biomedical Research Sandler Fellows Program (to R.L.JT.) for financial support. We would like to thank
231 Norma Neff and Michelle Tan for all the help with library quality control and sequencing.

232
233

233 **AUTHOR CONTRIBUTIONS:**

234 Conceptualization, R.L.B, D.L., A.D.T, S.D., and R.L.JT.; Methodology, R.L.B and A.M.; Validation, R.L.B. and D.L.;
235 Formal Analysis, R.L.B. and D.L.; Investigation, R.L.B, D.L., and A.M; Resources, U.E.L., A.S., V.PP, L.B., and A.D.T.;
236 Data Curation: D.L., and A.M.; Writing – Original Draft, R.L.B and R.L.JT.; Writing – Review & Editing, D.L., A.M.,
237 U.E.L. and S.D.; Visualization, R.L.B. and D.L.; Supervision, S.D. and R.L.JT.; Funding Acquisition, S.D. and R.L.JT.

238
239

239 **REFERENCES**

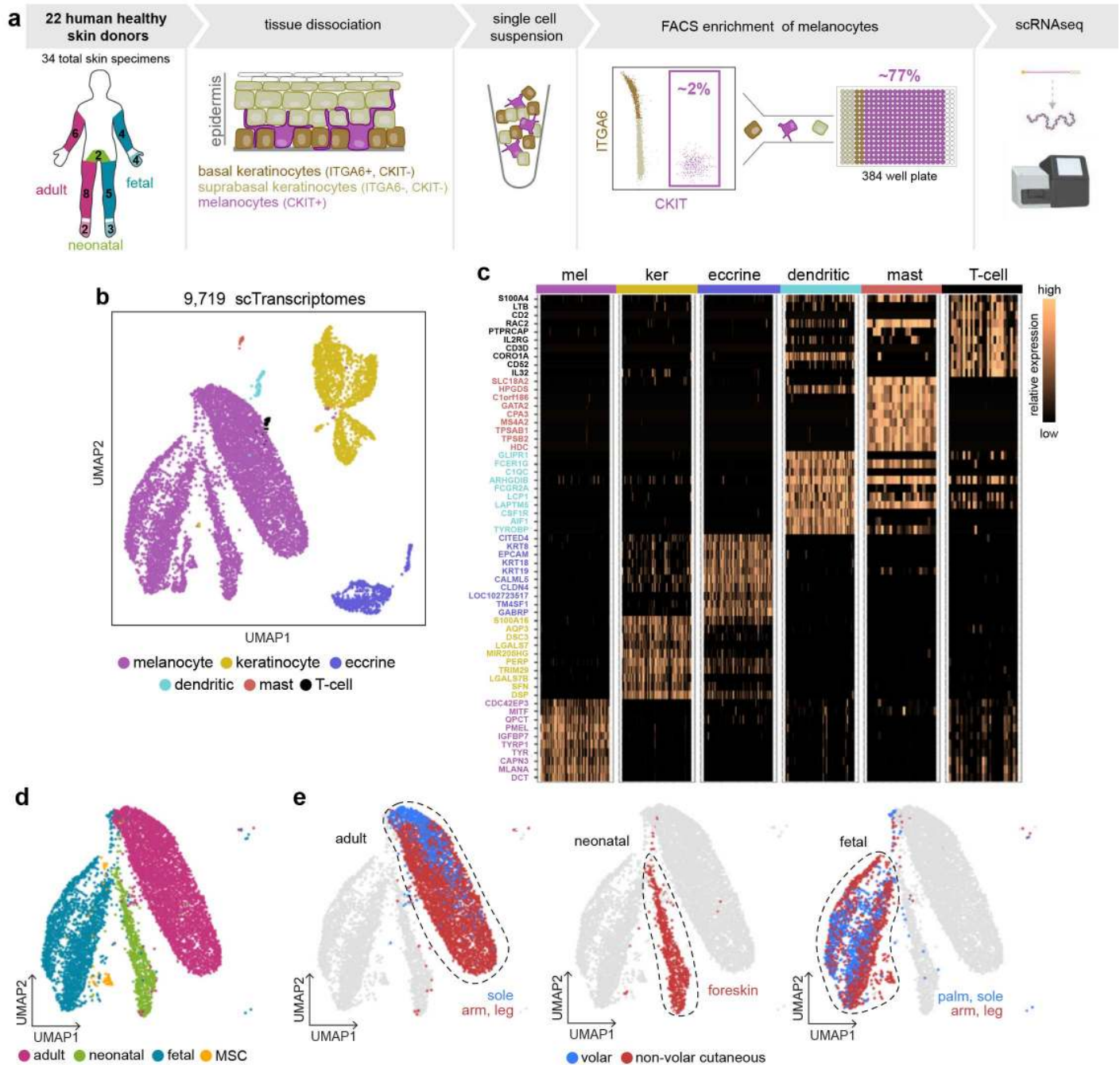
- 240 1. Hou, L., Arnheiter, H. & Pavan, W. J. Interspecies difference in the regulation of melanocyte development
241 by SOX10 and MITF. *Proc. Natl. Acad. Sci. U. S. A.* **103**, 9081–9085 (2006).
- 242 2. Adameyko, I. *et al.* Schwann Cell Precursors from Nerve Innervation Are a Cellular Origin of Melanocytes in
243 Skin. *Cell* **139**, 366–379 (2009).
- 244 3. Mort, R. L., Jackson, I. J. & Elizabeth Patton, E. The melanocyte lineage in development and disease.
245 *Development (Cambridge)* vol. 142 620–632 (2015).
- 246 4. Yamaguchi, Y. *et al.* Mesenchymal-epithelial interactions in the skin: Increased expression of dickkopf1 by
247 palmo-plantar fibroblasts inhibits melanocyte growth and differentiation. *J. Cell Biol.* **165**, 275–285 (2004).
- 248 5. Hayward, N. K. *et al.* Whole-genome landscapes of major melanoma subtypes. *Nature* **545**, 175–180
249 (2017).
- 250 6. Rabbie, R., Ferguson, P., Molina-Aguilar, C., Adams, D. J. & Robles-Espinoza, C. D. Melanoma subtypes:
251 genomic profiles, prognostic molecular markers and therapeutic possibilities. *Journal of Pathology* vol. 247
252 539–551 (2019).
- 253 7. Malta, T. M. *et al.* Machine Learning Identifies Stemness Features Associated with Oncogenic
254 Dedifferentiation. *Cell* **173**, 338–354.e15 (2018).
- 255 8. Gupta, P. B. *et al.* The melanocyte differentiation program predisposes to metastasis after neoplastic
256 transformation. *Nat. Genet.* **37**, 1047–1054 (2005).
- 257 9. Belote, R. L. & Simon, S. M. Ca²⁺ transients in melanocyte dendrites and dendritic spine-like structures
258 evoked by cell-to-cell signaling. *J. Cell Biol.* **219**, (2020).
- 259 10. NORRIS, A., TODD, C., GRAHAM, A., QUINN, A. G. & THODY, A. J. The expression of the c-kit receptor by
260 epidermal melanocytes may be reduced in vitiligo. *Br. J. Dermatol.* **134**, 299–306 (1996).
- 261 11. Randall, V. A., Jenner, T. J., Hibberts, N. A., De Oliveira, I. O. & Vafaei, T. Stem cell factor/c-Kit signalling in
262 normal and androgenetic alopecia hair follicles. *J. Endocrinol.* **197**, 11–23 (2008).
- 263 12. Picelli, S. *et al.* Smart-seq2 for sensitive full-length transcriptome profiling in single cells. *Nat. Methods* **10**,
264 1096–1100 (2013).

- 265 13. Hsiao, C. J. *et al.* Characterizing and inferring quantitative cell cycle phase in single-cell RNA-seq data
266 analysis. *bioRxiv* 526848 (2019) doi:10.1101/526848.
- 267 14. Yamaguchi, Y. *et al.* Epithelial-mesenchymal interactions in wounds: treatment of palmoplantar wounds by
268 nonpalmoplantar pure epidermal sheet grafts. *Arch. Dermatol.* **137**, 621–8 (2001).
- 269 15. Joshi, S. S. *et al.* CD34 defines melanocyte stem cell subpopulations with distinct regenerative properties.
270 *PLOS Genet.* **15**, e1008034 (2019).
- 271 16. Marie, K. L. *et al.* Melanoblast transcriptome analysis reveals pathways promoting melanoma metastasis.
272 *Nat. Commun.* **11**, 1–18 (2020).
- 273 17. Rezza, A. *et al.* Signaling Networks among Stem Cell Precursors, Transit-Amplifying Progenitors, and their
274 Niche in Developing Hair Follicles. *Cell Rep.* **14**, 3001–3018 (2016).
- 275 18. Sennett, R. *et al.* An Integrated Transcriptome Atlas of Embryonic Hair Follicle Progenitors, Their Niche, and
276 the Developing Skin. *Dev. Cell* **34**, 577–591 (2015).
- 277 19. Mica, Y., Lee, G., Chambers, S. M., Tomishima, M. J. & Studer, L. Modeling Neural Crest Induction,
278 Melanocyte Specification, and Disease-Related Pigmentation Defects in hESCs and Patient-Specific iPSCs.
279 *Cell Rep.* **3**, 1140–1152 (2013).
- 280 20. Tsoi, J. *et al.* Multi-stage Differentiation Defines Melanoma Subtypes with Differential Vulnerability to
281 Drug-Induced Iron-Dependent Oxidative Stress. *Cancer Cell* **33**, 890-904.e5 (2018).
- 282 21. Hoek, K. S. *et al.* In vivo switching of human melanoma cells between proliferative and invasive states.
283 *Cancer Res.* **68**, 650–656 (2008).
- 284 22. Richard, G. *et al.* ZEB 1-mediated melanoma cell plasticity enhances resistance to MAPK inhibitors. *EMBO*
285 *Mol. Med.* **8**, 1143–1161 (2016).
- 286 23. Landsberg, J. *et al.* Melanomas resist T-cell therapy through inflammation-induced reversible
287 dedifferentiation. *Nature* **490**, 412–416 (2012).
- 288 24. Grzywa, T. M., Paskal, W. & Włodarski, P. K. Intratumor and Intertumor Heterogeneity in Melanoma.
289 *Translational Oncology* vol. 10 956–975 (2017).
- 290 25. Jerby-Arnon, L. *et al.* A Cancer Cell Program Promotes T Cell Exclusion and Resistance to Checkpoint
291 Blockade. *Cell* **175**, 984-997.e24 (2018).
- 292 26. Tirosh, I. *et al.* Dissecting the multicellular ecosystem of metastatic melanoma by single-cell RNA-seq.
293 *Science (80-)*. **352**, 189–196 (2016).
- 294 27. Raskin, L. *et al.* Transcriptome profiling identifies HMGA2 as a biomarker of melanoma progression and
295 prognosis. *J. Invest. Dermatol.* **133**, 2585–2592 (2013).
- 296 28. Guo, B. *et al.* Humanin peptide suppresses apoptosis by interfering with Bax activation. *Nature* **423**, 456–
297 461 (2003).
- 298 29. Newman, A. M. *et al.* Robust enumeration of cell subsets from tissue expression profiles. *Nat. Methods* **12**,
299 453–457 (2015).
- 300 30. Akbani, R. *et al.* Genomic Classification of Cutaneous Melanoma. *Cell* **161**, 1681–1696 (2015).
- 301 31. Wishart, D. S. *et al.* DrugBank 5.0: A major update to the DrugBank database for 2018. *Nucleic Acids Res.*
302 **46**, D1074–D1082 (2018).
- 303 32. Hayward, N. K. *et al.* Whole-genome landscapes of major melanoma subtypes. *Nature* **545**, 175–180
304 (2017).
- 305 33. Goydos, J. S. & Shoen, S. L. Acral lentiginous melanoma. in *Cancer Treatment and Research* vol. 167 321–
306 329 (Kluwer Academic Publishers, 2016).
- 307 34. Okamoto, N. *et al.* A melanocyte-melanoma precursor niche in sweat glands of volar skin. *Pigment Cell*
308 *Melanoma Res.* **27**, 1039–1050 (2014).
- 309 35. Siegel, R. L., Miller, K. D. & Jemal, A. Cancer statistics, 2020. *CA. Cancer J. Clin.* **70**, 7–30 (2020).
- 310 36. Lezcano, C., Jungbluth, A. A., Nehal, K. S., Hollmann, T. J. & Busam, K. J. PRAME Expression in Melanocytic
311 Tumors. *Am. J. Surg. Pathol.* **42**, 1456–1465 (2018).
- 312 37. Drey, E. A., Kang, M. S., McFarland, W. & Darney, P. D. Improving the accuracy of fetal foot length to
313 confirm gestational duration. *Obstet. Gynecol.* **105**, 773–778 (2005).
- 314 38. Dobin, A. *et al.* STAR: Ultrafast universal RNA-seq aligner. *Bioinformatics* **29**, 15–21 (2013).
- 315 39. Anders, S., Pyl, P. T. & Huber, W. HTSeq-A Python framework to work with high-throughput sequencing
316 data. *Bioinformatics* **31**, 166–169 (2015).
- 317 40. Wolf, F. A., Angerer, P. & Theis, F. J. SCANPY: Large-scale single-cell gene expression data analysis. *Genome*

- 318 *Biol.* **19**, 15 (2018).
- 319 41. Hsiao, C. J. *et al.* Characterizing and inferring quantitative cell cycle phase in single-cell RNA-seq data
320 analysis. *Genome Res.* **30**, 611–621 (2020).
- 321 42. Liu, J. *et al.* An Integrated TCGA Pan-Cancer Clinical Data Resource to Drive High-Quality Survival Outcome
322 Analytics. *Cell* **173**, 400–416.e11 (2018).
- 323 43. Gleason, B. C., Crum, C. P. & Murphy, G. F. Expression patterns of MITF during human cutaneous
324 embryogenesis: Evidence for bulge epithelial expression and persistence of dermal melanoblasts. *J. Cutan.*
325 *Pathol.* **35**, 615–622 (2008).
- 326 44. Holbrook, K. A., Underwood, R. A., Vogel, A. M., Gown, A. M. & Kimball, H. The appearance, density and
327 distribution of melanocytes in human embryonic and fetal skin revealed by the anti-melanoma monoclonal
328 antibody, HMB-45. *Anat. Embryol. (Berl.)*. **180**, 443–455 (1989).
- 329 45. Saxena, N., Mok, K. W. & Rendl, M. An updated classification of hair follicle morphogenesis. *Experimental*
330 *Dermatology* vol. 28 332–344 (2019).
- 331 46. Nishikawa, S.-I. & Osawa, M. Generating quiescent stem cells. *Pigment cell Res.* **20**, 263–70 (2007).
- 332 47. Denecker, G. *et al.* Identification of a ZEB2-MITF-ZEB1 transcriptional network that controls melanogenesis
333 and melanoma progression. *Cell Death Differ.* **21**, 1250–61 (2014).
- 334 48. Lu, R. *et al.* Transcription factor TCF4 maintains the properties of human corneal epithelial stem cells. *Stem*
335 *Cells* **30**, 753–761 (2012).
- 336 49. Li, Z., Li, Y. & Jiao, J. Neural progenitor cells mediated by H2A.Z.2 regulate microglial development via
337 Cxcl14 in the embryonic brain. *Proc. Natl. Acad. Sci. U. S. A.* **116**, 24122–24132 (2019).
- 338 50. Mica, Y., Lee, G., Chambers, S. M., Tomishima, M. J. & Studer, L. Modeling Neural Crest Induction,
339 Melanocyte Specification, and Disease-Related Pigmentation Defects in hESCs and Patient-Specific iPSCs.
340 *Cell Rep.* **3**, 1140–1152 (2013).
- 341 51. Osawa, M. *et al.* Molecular characterization of melanocyte stem cells in their niche. *Development* **132**,
342 5589–5599 (2005).
- 343 52. Lu, Z. *et al.* Hair follicle stem cells regulate retinoid metabolism to maintain the self-renewal niche for
344 melanocyte stem cells. *Elife* **9**, (2020).
- 345 53. Widmer, D. S. *et al.* Systematic classification of melanoma cells by phenotype-specific gene expression
346 mapping. *Pigment Cell Melanoma Res.* **25**, 343–353 (2012).
- 347 54. Strub, T. *et al.* Essential role of microphthalmia transcription factor for DNA replication, mitosis and
348 genomic stability in melanoma. *Oncogene* **30**, 2319–2332 (2011).
- 349 55. Akbani, R. *et al.* Genomic Classification of Cutaneous Melanoma. *Cell* **161**, 1681–1696 (2015).
- 350 56. Cirenajwis, H. *et al.* Molecular stratification of metastatic melanoma using gene expression profiling -
351 Prediction of survival outcome and benefit from molecular targeted therapy. *Oncotarget* **6**, 12297–12309
352 (2015).
- 353 57. Rambow, F. *et al.* Toward Minimal Residual Disease-Directed Therapy in Melanoma. *Cell* **174**, 843-855.e19
354 (2018).
- 355
- 356
- 357
- 358
- 359
- 360
- 361
- 362
- 363
- 364
- 365
- 366
- 367
- 368
- 369
- 370

371
372

Figure 1



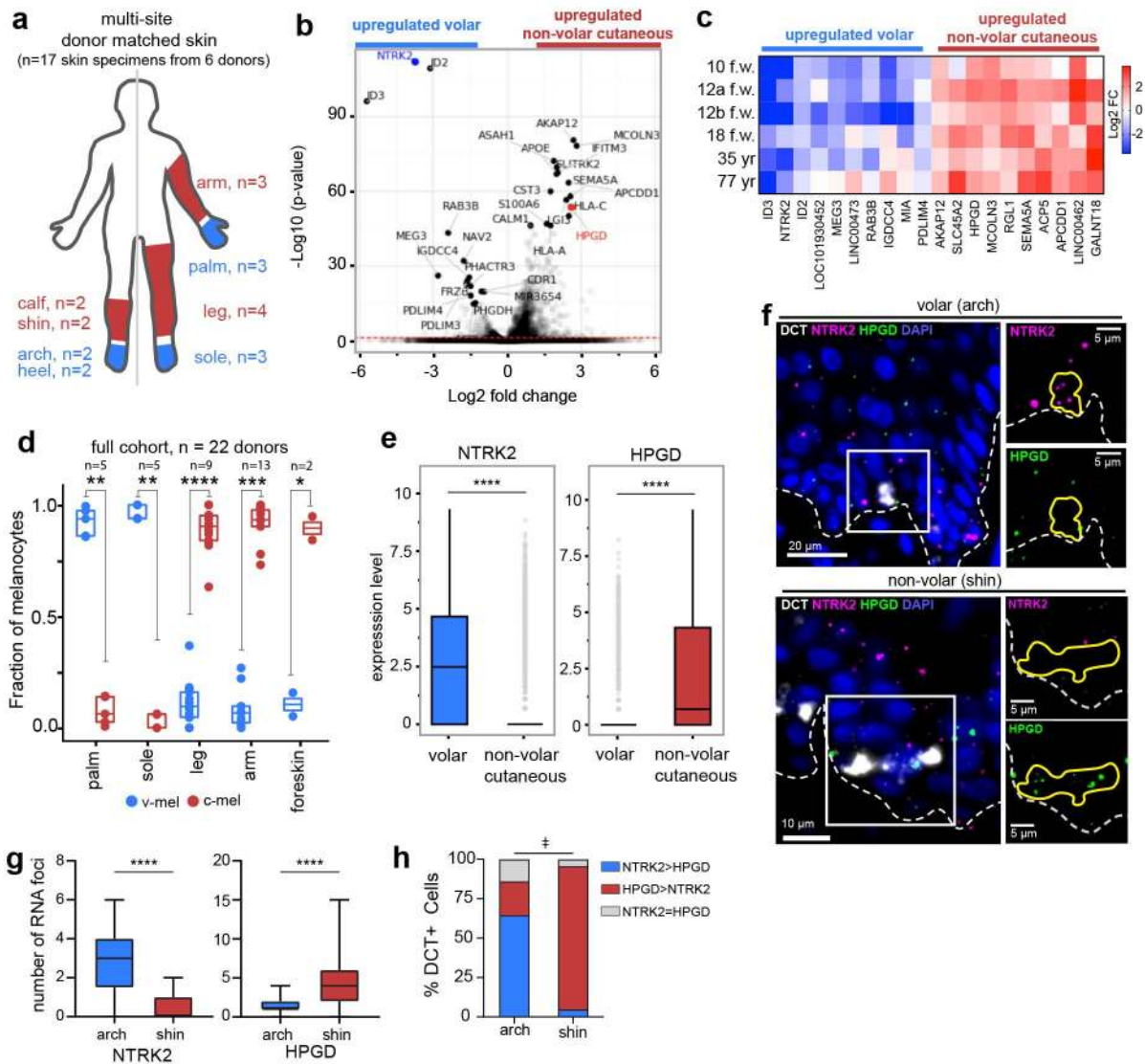
373
374

Figure 1: Melanocyte transcriptomic profiles differ based on development and anatomic location. a) Fresh from healthy human skin single cell isolation, enrichment, and sequencing pipeline. **b)** UMAP visualization of the 9,719 cells (7088 melanocytes, 1865 keratinocytes, 636 eccrine, 76 dendritic, 25 mast, and 29 T-cells) that passed quality control colored by cell types identified from Louvain clustering and candidate genes. **c)** Heat map showing the relative expression of top differentially expressed genes for each cluster in (b). **d)** UMAP of all non-cycling melanocytes with developmental age and fetal MSC annotation based on Louvain clustering (see also Extended Data Fig. 3). **e)** Fetal and adult melanocytes segregate by anatomic location.

382
383
384
385
386

387
388

Figure 2



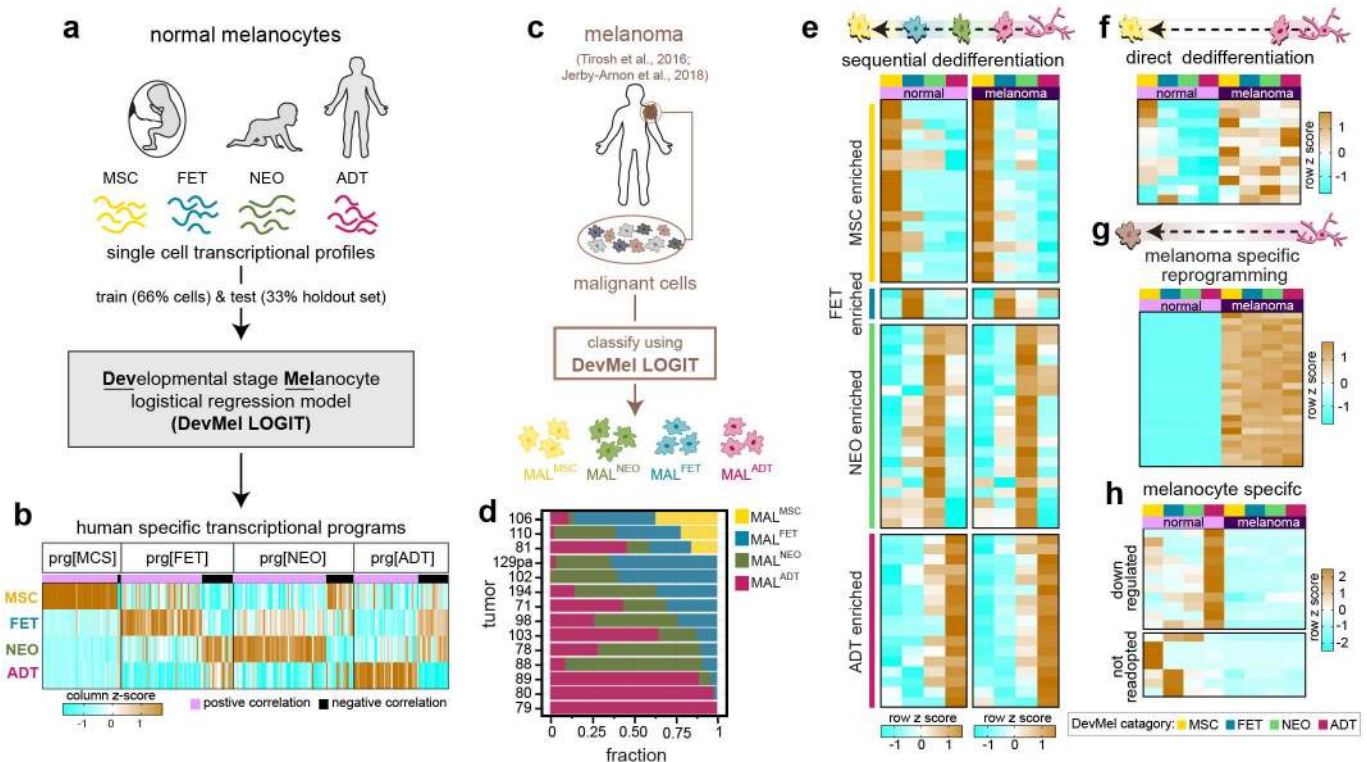
389
390

Figure 2: Anatomic site-specific melanocyte sub-population enrichment arises during development and persists in adulthood. **a)** Schematic illustrating cohort of donor-matched non-volar and volar skin. n = 6 donors and 17 total skin specimens. See also Extended Data Table 1. **b)** Volcano plot of genes enriched in non-volar cutaneous vs volar melanocytes. See also Supplementary Table 2. **c)** Top site-specific differentially expressed genes (DEGs), largest median per-patient log-fold-change between volar and non-volar melanocytes, among donor matched samples. **d)** Fraction of melanocytes with v-mel or c-mel signature in each skin specimen (n= 34) from all 22 patients. Two-sided Mann-Whitney U test with Bonferroni multiple testing correction, * p-value = 0.12, ** p-value <0.01, ***p-value < 0.001, ****p-value < 0.0001. **e)** Expression level of v-mel gene, *NTRK2*, and c-mel gene, *HPGD*, in volar melanocytes (sole, palm) compared to non-volar cutaneous melanocytes (arm, leg). Two-sided Mann-Whitney U test, ****p-value < 0.0001. Interquartile range with median, standard deviation, and outliers (grey circles). **f)** Representative pseudo-colored fluorescent microscopy images from RNAscope staining for *NTRK2*, *HPGD*, and the melanocyte marker *DCT* in adult volar and non-volar epidermis. Dashed line, epidermal-dermal melanocytes in volar (arch) and non-volar cutaneous skin (shin) in (f). Interquartile range, 5-95%, and outliers. Two-tailed unpaired t-test ****p-value < 0.0001 **h)** The percent v-mel (*NTRK2* > *HPGD*) and c-mel (*HPGD* > *NTRK2*) at each site in (f) showing volar skin has a significantly higher proportion of v-mels compared to non-volar cutaneous skin and non-volar cutaneous skin has a significantly higher proportion of c-mels compared to volar skin (‡, Two-sample Z-test for proportions, v-mel: z = 6.062, p-value = 1.8e-11, and c-mel: z = 7.885, p-value = 1.6e-15). For (g) and (h) n= 44 cells from arch and n = 22 cells from shin.

408
409

410
411

Figure 3



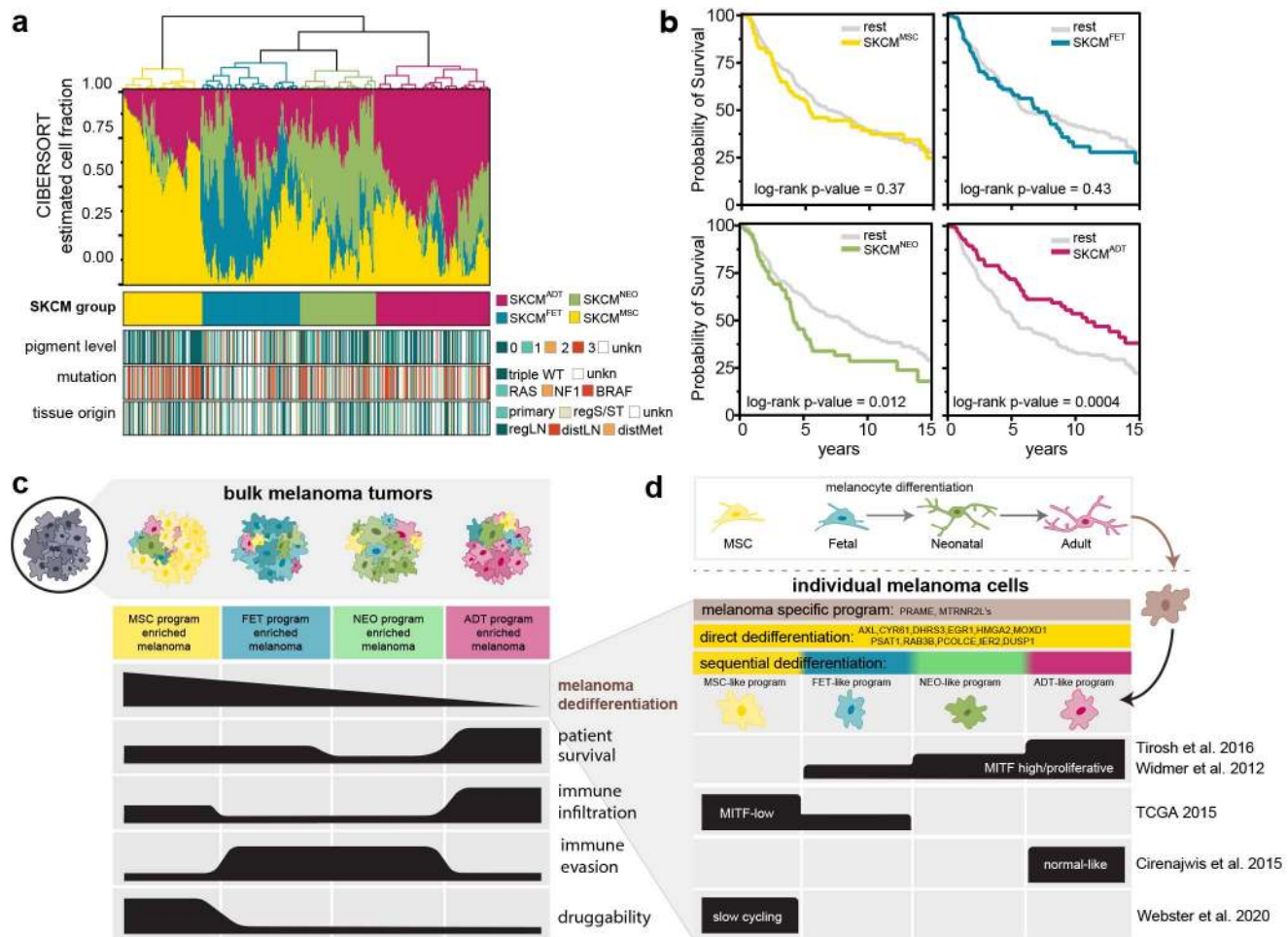
412
413
414
415
416
417
418
419
420
421
422
423
424
425
426
427
428
429
430
431
432
433
434
435
436
437
438
439
440
441
442

Figure 3: Identification of distinct patterns of developmental programs required in metastasized melanomas.

a) Schematic of the Developmental stage Melanocyte logistical regression model (DevMel LOGIT) used to generate and validate unique transcription profiles for each developmental stage of normal human melanocytes. **b)** Heatmap of the relative expression (column z score) of genes in each DevMel program (prg) from (a). See also Extended Data Fig. 7 and Supplementary Table 4 for gene list. **c)** DevMel LOGIT was used to classify individual melanoma cells by normal melanocyte developmental stages. Every melanoma cell (MAL) was categorized by the predominantly expressed developmental stage program. **d)** Individual tumors are a heterogeneous mix of malignant cells in different dedifferentiation states. Fraction of MAL^{ADT}, MAL^{NEO}, MAL^{FET} and MAL^{MSC} cells in each of the 14 tumors analyzed from Tirosh *et al.* and Jerby-Arnon *et al.* in (c). **e-h)** Dedifferentiation can occur through several categories of cancer-associated transcriptional reprogramming: **e)** sequential dedifferentiation, a reverse stepwise unfolding of development; **f)** direct dedifferentiation, direct reacquisition of programs from early developmental stages; **g)** melanoma specific, acquisition of programs not associated with the stages of melanocyte development identified here. **h)** Normal adult developmental stage programs that are lost and earlier developmental stage programs not readopted in metastatic melanoma. Examples of each category are visualized as heatmaps of the relative expression (row z score). See Supplemental Table 5 for complete gene lists.

443
444

Figure 4

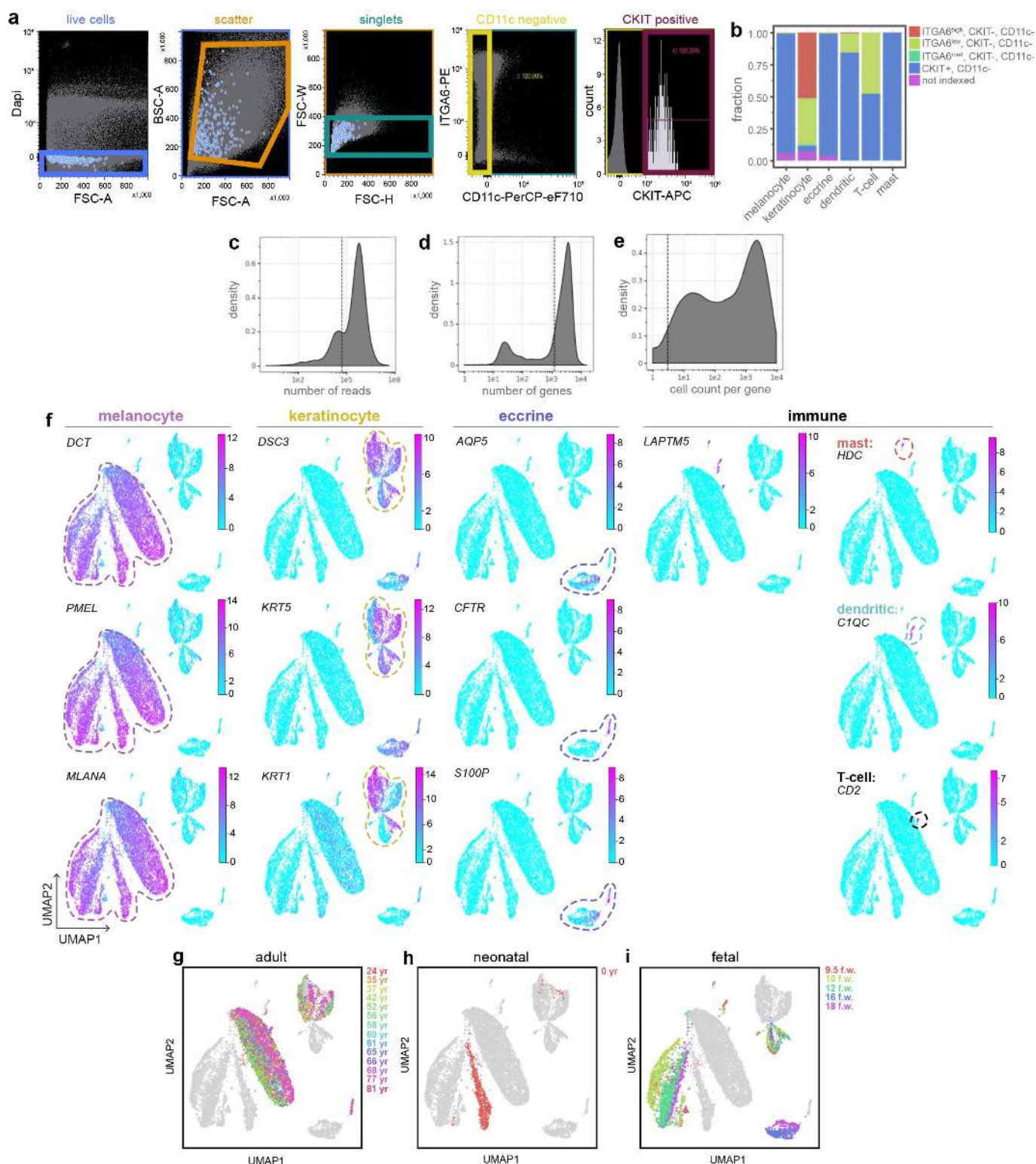


445
446
447
448
449
450
451
452
453
454
455
456
457
458
459
460
461
462
463
464
465
466
467
468

Figure 4: Reacquisition of specific developmental programs in heterogeneous melanoma metastases is prognostic. **a)** Hierarchical clustering of TCGA SKCM tumors based on fractional composition of normal melanocyte developmental stages assigned using CIBERSORT (top) with clinicopathological features (bottom panels). **b)** Kaplan Meier curves for each SKCM group from (a). Enrichment for cells similar to ADT is associated with increased survival, whereas enrichment for NEO is associated with worse survival. **c-d)** Schematic summarizing the decoding of melanoma dedifferentiation using human developmental programs. **c)** Individual melanoma tumors are comprised of a heterogeneous mix of malignant cells expressing defined melanocyte developmental programs. The fraction of cells expressing each program within the tumor is predictive of overall survival and correlates to signatures of immune infiltration, evasion and potential therapeutic options. **d)** Each melanoma cell can occupy a different degree of dedifferentiation defined by sequential dedifferentiation transcriptional programs (Fig. 3 and Supplementary Table 5). The MSC- and adult-like programs are associated with previously described melanoma signatures whereas the fetal- and neonatal-like programs do not segregate with known melanoma signatures offering unique insight into previously uncharacterized melanoma transcriptional states (Extended Data Fig. 8). Genes common to all cells include melanoma specific genes, such as PRAME, or direct reprogramming to an early developmental stage (direct dedifferentiation).

469
470

Extended Data Figure 1

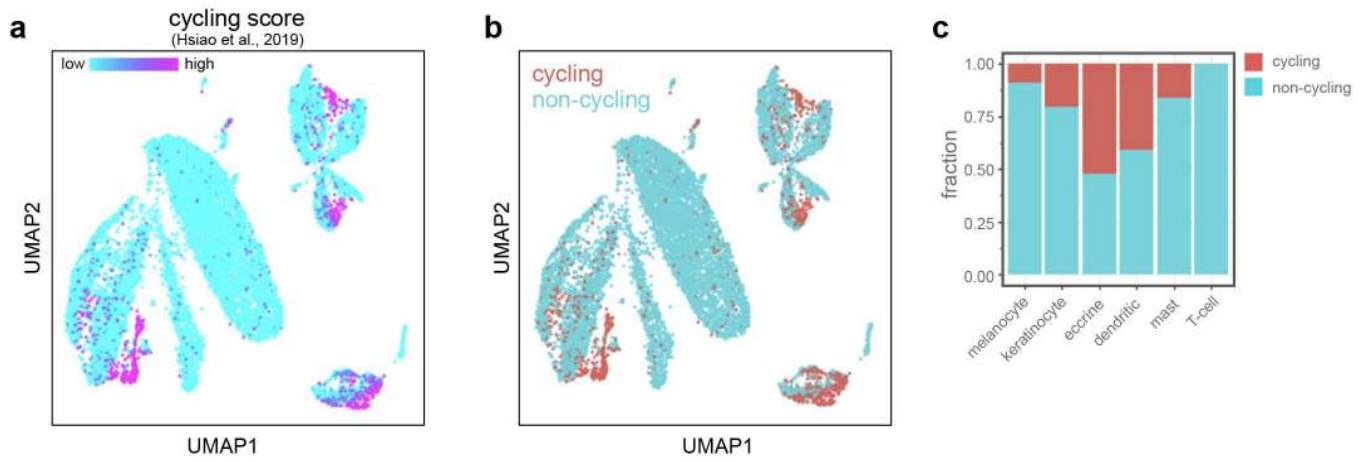


471
472
473
474
475
476
477
478
479

Extended Data Figure 1: Single cell RNA sequencing quality control, cell-type specific markers, and donor age. a) FACS gate protocol for representative sort. Melanocytes (blue circles in live, scatter, and singlets) were isolated as CKIT+ cells from the CD11c- gate. **b)** Fraction of cells from each indexed FACS gate assignment. **c)** Number of reads and **d)** number of genes per cell for all 14,370 sequenced cells. Dashed line: quality control threshold, cells with < 50,000 reads and < 500 genes were excluded from further analysis. **e)** Genes expressed in more than 3 cells (dashed line) were included for subsequent analysis. **f)** Cell-type specific gene expression overlay on UMAPs. Genes indicated in upper left corner of each plot. **g-i)** UMAP with donor age overlay for **g)** adult, **h)** neonatal, and **i)** fetal cells.

480
481

Extended Data Figure 2



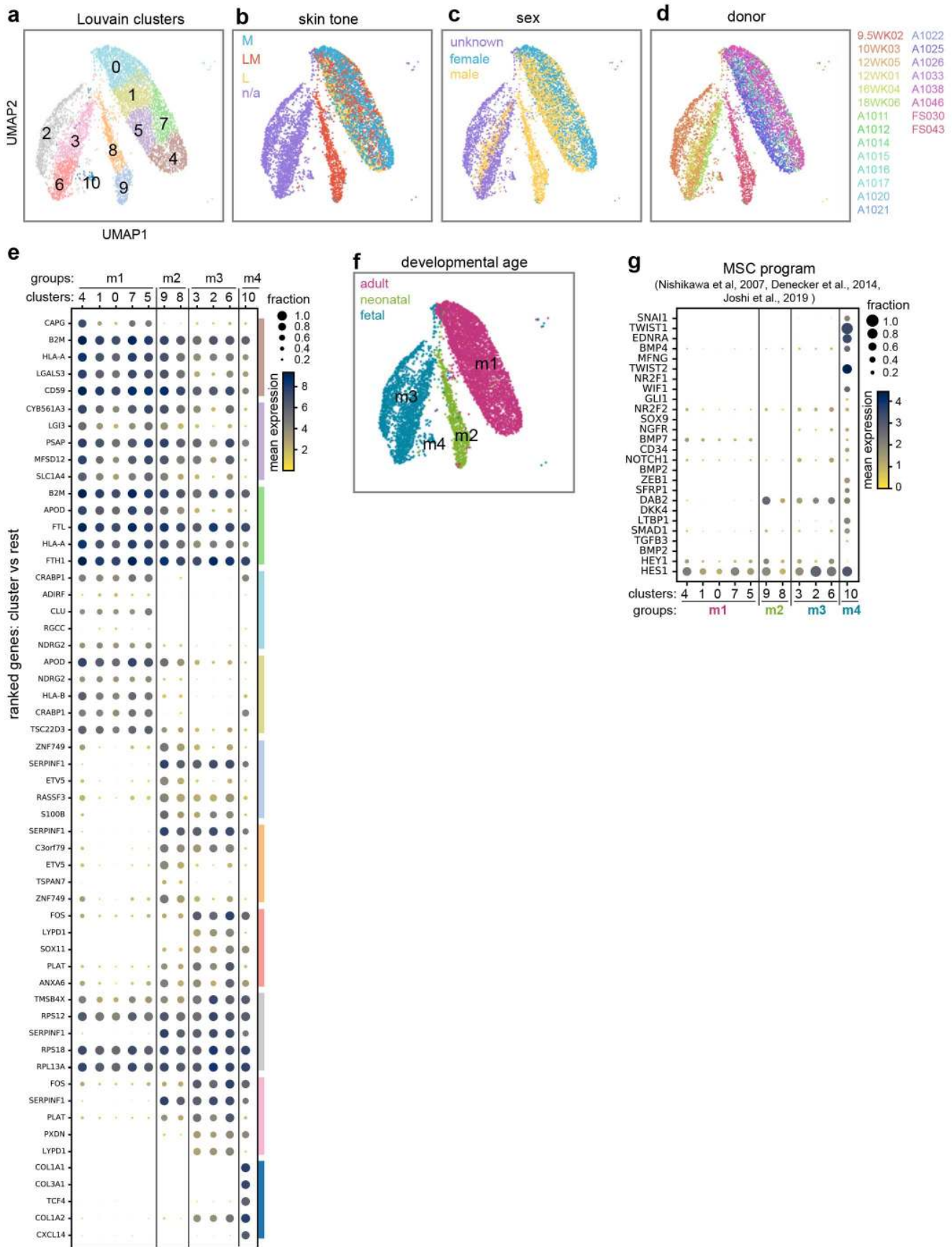
482
483

Extended Data Figure 2: Characterization of cell cycle state. a) UMAP projection of cycling cell program score used to determine which cells were designated as **b)** cycling (blue, in G2 & M phase) vs non-cycling (red). **c)** Fraction of cycling and non-cycling cells for each cell type identified in Fig. 1.

484
485
486
487
488
489
490
491
492
493
494
495
496
497
498
499
500
501
502
503
504
505
506
507
508
509
510
511
512
513
514
515
516
517
518
519
520

521

Extended Data Figure 3



522

523

524

525

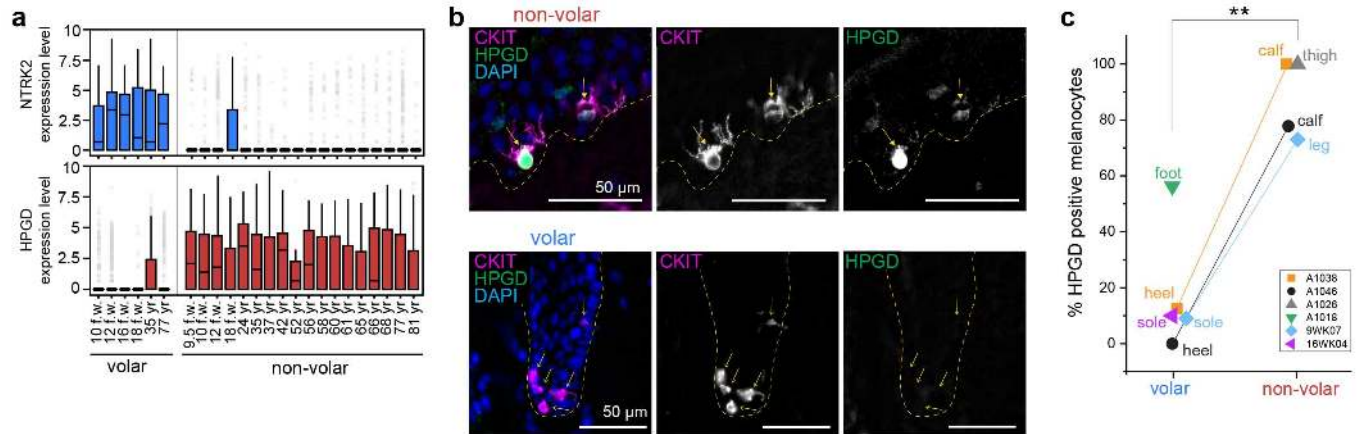
Extended Data Figure 3: Identification and characterization of melanocyte clusters. a) UMAP of melanocytes showing Louvain clusters do not correspond to b) skin tone, c) sex, or d) donor. e) Dotplot of the mean expression and fraction of cells expressing the top 5 ranked genes (Wilcoxon Rank-sum) for each Louvain cluster in (a). Clusters

526 with similar ranked gene expression patterns were bin into four groups: m1 (clusters 4,1,0,7,5), m2 (clusters 9,8),
527 m3 (clusters 3,2,6), and m4 (cluster 10). **f)** Group m1 was comprised of adult melanocytes and m2 neonatal
528 melanocytes, whereas groups m3 and m4 were comprised of fetal melanocytes. **g)** Dotplot showing group m4,
529 from fetal hair-bearing non-volar cutaneous skin (see Fig. 1e), expresses known melanocyte stem cell (MSC) markers.
530 Groups are colored by developmental age in (f).

531
532
533
534
535
536
537
538
539
540
541
542
543
544
545
546
547
548
549
550
551
552
553
554
555
556
557
558
559
560
561
562
563
564
565
566
567
568
569
570
571
572
573
574
575
576
577
578

579
580

Extended Data Figure 4



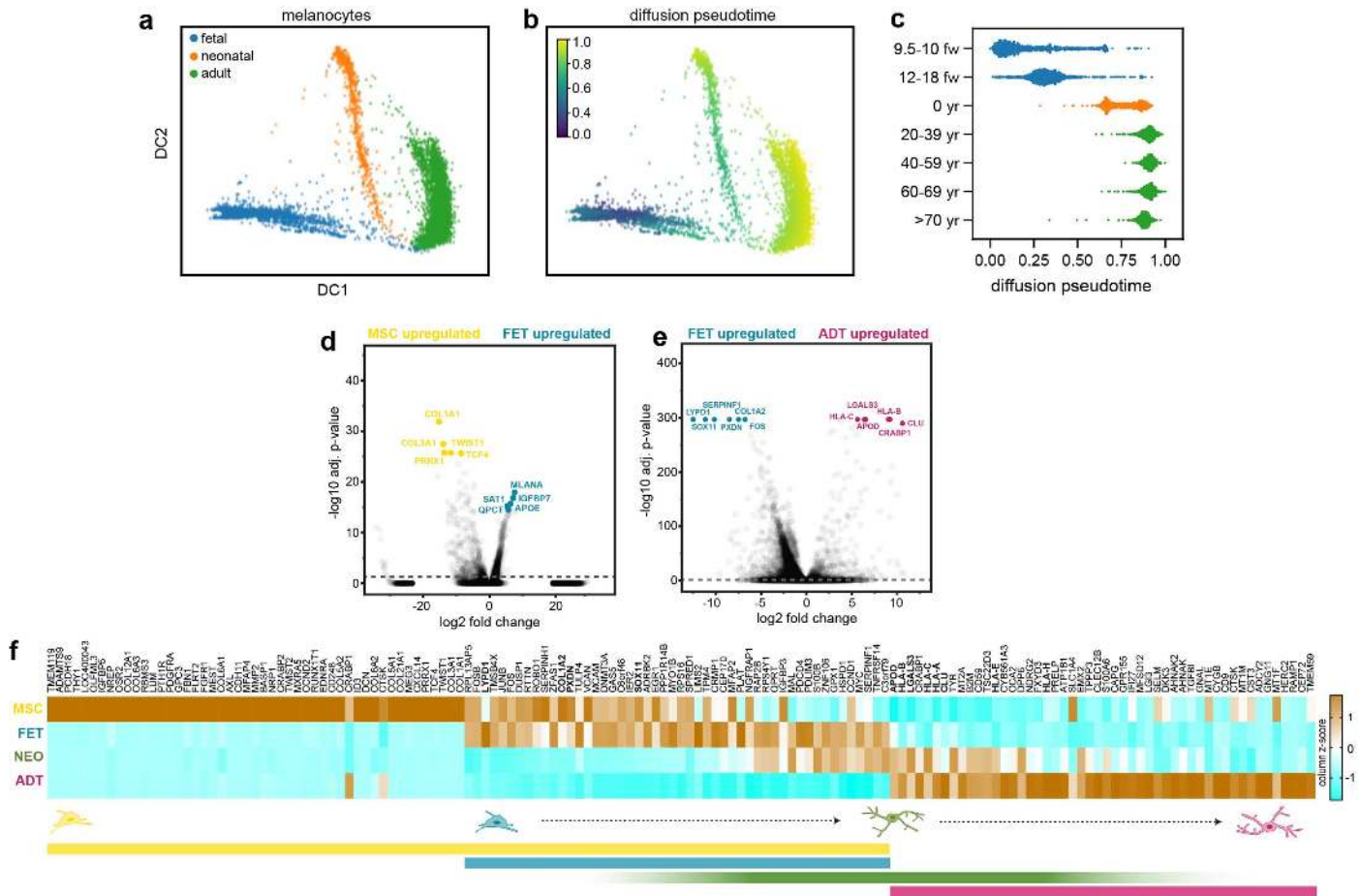
581
582
583
584
585
586
587
588
589
590
591
592
593
594
595
596
597
598
599
600
601
602
603
604
605
606
607
608
609
610
611
612
613
614
615
616
617
618
619
620

Extended Data Figure 4: Validation of v-mel and c-mel site-specific enrichment in adult and fetal skin.

a) Expression level of v-mel gene, *NTRK2*, and c-mel gene, *HPGD*, in volar melanocytes compared to non-volar cutaneous melanocytes at each age (n=22 donors). Interquartile range with median, standard deviation, and outliers (grey circles). **b**) Immunofluorescence co-staining of adult volar and non-volar skin cryo-sections with the c-mel marker *HPGD* (green) and melanocyte marker *CKIT* (magenta). Dashed line, epidermal-dermal junction. **c**) Quantification of site-specific enrichment of melanocyte c-mel and v-mel subclasses. Percent *HPGD* positive melanocytes per donor volar and non-volar skin. Adult skin: A1046, n=78 total cells; A1038, n = 39 total cells; A1018, n = 48 total cells; A1026, n= 15 total cells. Fetal skin: 9WK07, n = 41 total cells; 16WK04, n = 10 total cells. Two-tailed unpaired t-test, ** p-value = 0.001.

621
622

Extended Data Figure 5

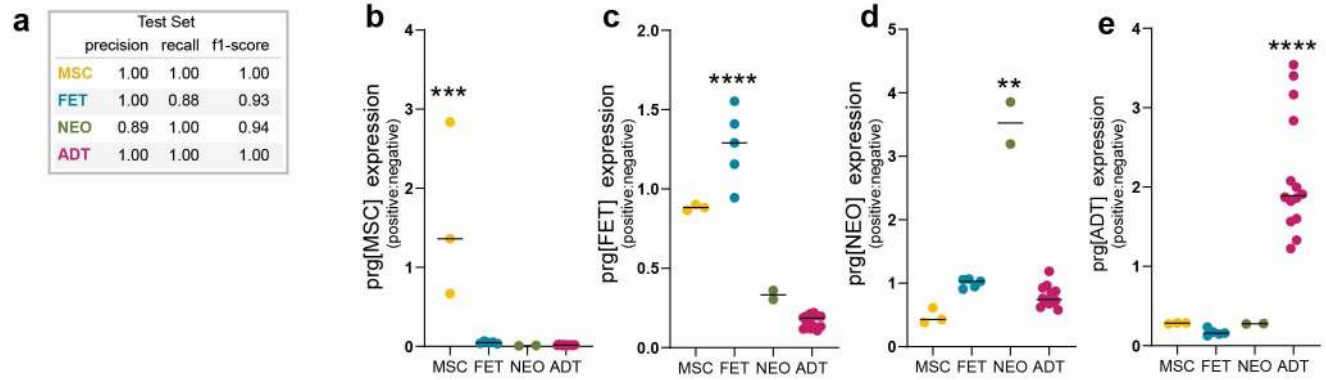


623
624
625
626
627
628
629
630
631
632
633
634
635
636
637
638
639
640
641
642
643
644
645
646
647
648

Extended Data Figure 5: Pseudotime and pairwise differential expression analysis of developmental ages and groups. **a)** Melanocytes cluster by developmental age in diffusion component space DC1 and DC2. **b)** Pseudotime overlay onto DC space. **c)** Progression from fetal to adult through an intermediate neonatal transcriptional state. **d)** Volcano plot showing the top ten DEGs between MSC (yellow) and FET (teal) non-volar cutaneous melanocyte populations. **e)** Volcano plot showing the top ten DEGs between FET (teal) and ADT (magenta) non-volar cutaneous melanocytes. **f)** Heatmap visualization of the relative expression (column z score) of DEGs from (d) and (e) for all four non-volar cutaneous developmental groups. Both MSC and FET were enriched for known developmental genes (SOX11, LYPD1) and genes involved in extracellular matrix establishment/remodeling (COL1A2, PXDN). The ADT group expressed genes involved in innate immunity, inflammation and regulating apoptosis/cell stress in other cell types and tissues (HLAs, APOD, CLU, LGALS3). The NEO group exhibited high expression of a subset of genes from both the FET and ADT stages, consistent with neonatal melanocytes being an intermediate developmental state. See Supplementary Table 3 for the full list.

649
650

Extended Data Figure 6



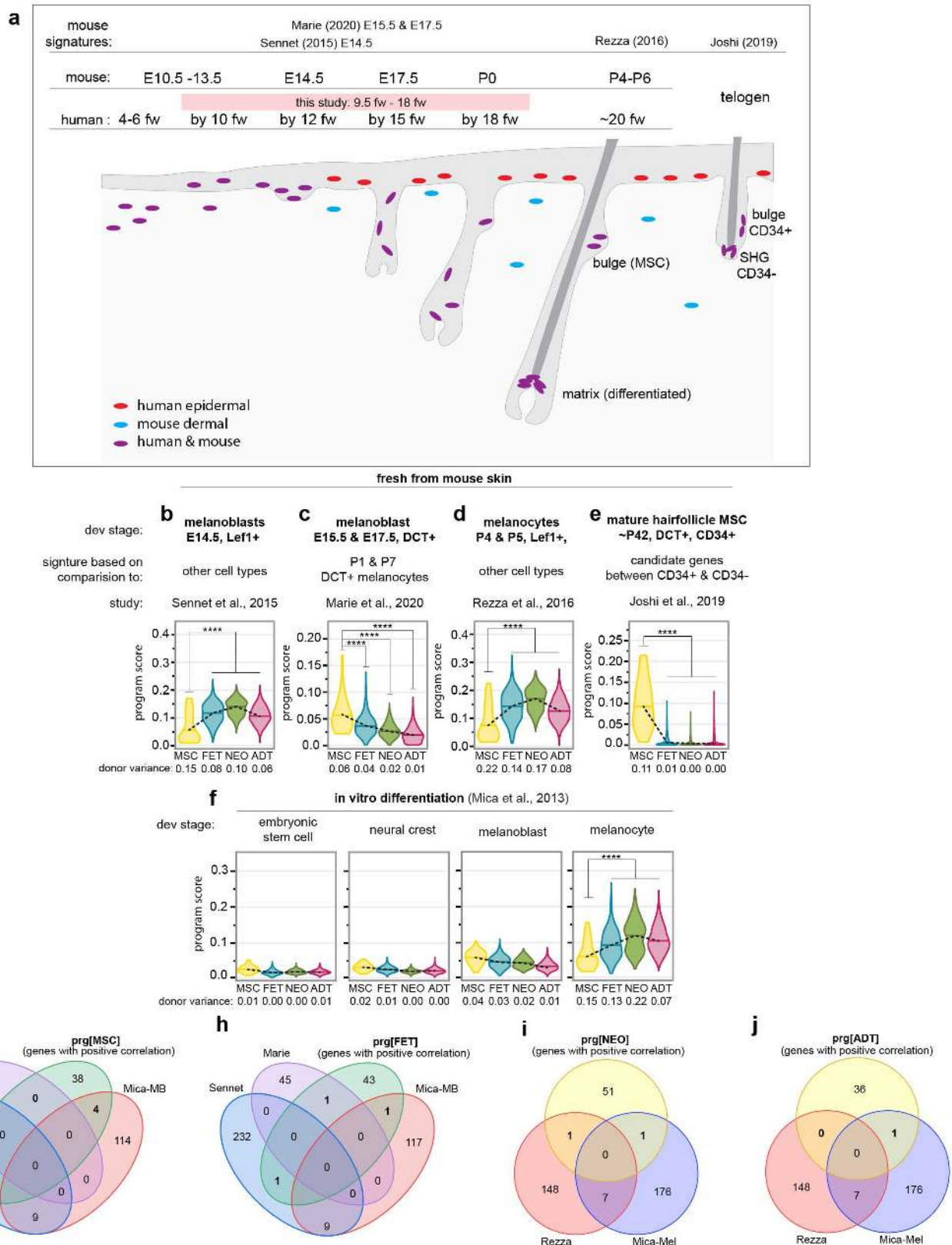
651
652

Extended Data Figure 6: Transcriptional profiling of human melanocyte differentiation. a) DevMel LOGIT classifier performance on hold out validation set. **b-e)** DevMel program expression is highly expressed by cells from all skin donors within each corresponding developmental stage. Program expression for each donor (black line, average) is the ratio of the mean expression of positively correlated genes and negatively correlated genes. Significant by one-sided Mann Whitney U test. **b)** prg[MSC]: MSC vs rest *** p-value = 0.0005, **c)** prg[FET]: FET vs rest **** p-value 0.0001, **d)** prg[NEO]: FET vs rest ** p-value = 0.0072, **e)** prg[ADT]: ADT vs rest **** p-value < 0.0001.

659
660
661
662
663
664
665
666
667
668
669
670
671
672
673
674
675
676
677
678
679
680
681
682
683
684
685
686
687
688
689
690
691

692
693

Extended Data Figure 7



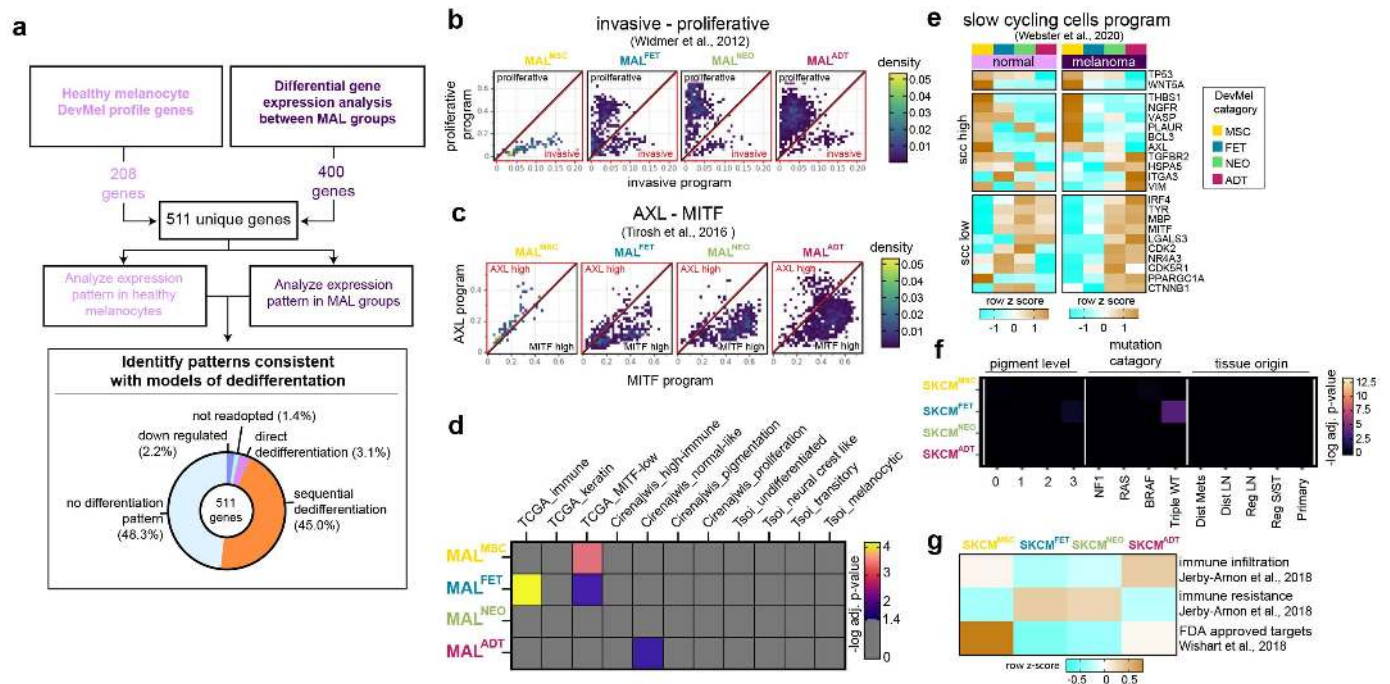
694
695
696
697
698
699
700

Extended Data Figure 7: Evaluation of model mammalian melanocyte developmental program expression in human non-volar cutaneous melanocyte developmental groups. **a)** Schematic summarizing human^{43,44} and corresponding mouse⁴⁵ melanocyte development captured in this study's dataset. In hair-bearing skin, both humans and mice develop follicular melanocytes (purple). Mice retain a dermal melanocyte population (blue) in fully developed skin, whereas humans develop resident epidermal melanocytes (red) within the skin at all anatomic locations. **b-f)** Violin plots show distribution of indicated transcriptional program expression scores for individual

701 cells within each developmental group MSC, FET, NEO, and ADT. Dashed line: mean expression. Program scores
702 were generated from published signatures of **b-c**) mouse melanoblasts (cell committed to the melanocyte fate)^{16,18},
703 **d**) melanocytes¹⁷, and **e**) melanocyte stem cells from mature hair follicles in adult mice¹⁵ and **f**) *in vitro* melanocyte
704 differentiation stages. For each individual cell, the program score is the mean normalized expression for all genes
705 in the indicated published gene signature. The variance of the average program expression among donors within
706 the MSC, FET, NEO, and ADT groups (reported below the corresponding group for each violin plot) was low showing
707 concordance across ages within each group. **** p-value < 1 x 10⁻⁷, significance determined by one-sided Man-
708 Whitney U test. **g-h**) Venn diagrams showing the number of unique and overlapping genes of melanoblast related
709 gene signatures with the positive correlated component of the DevMel profiles **g**) prg[MSC] and **h**) prg[FET]. **i-j**)
710 Venn diagrams showing the number of unique and overlapping genes of differentiated melanocyte related gene
711 signatures with the positively correlated component of the DevMel profiles **i**) prg[NEO] and **j**) prg[ADT].
712
713
714
715
716
717
718
719
720
721
722
723
724
725
726
727
728
729
730
731
732
733
734
735
736
737
738
739
740
741
742
743
744
745
746
747
748
749
750
751
752
753

754
755

Extended Data Figure 8



756
757

Extended Data Figure 8: Characterization of melanoma cells and tumors classified by *in situ* human melanocyte developmental programs. **a)** Workflow to generate gene set (511 unique genes) used to identify patterns associated with melanoma dedifferentiation (top). Percent of genes across MAL groups that exhibit patterns consistent with dedifferentiation categories in Fig. 3e-g. **b-c)** Density plots showing the expression of **b)** the Widmer *et al.* invasive and proliferative programs and **c)** the Tirosh *et al.* AXL and MITF programs for individual cells in MAL^{ADT}, MAL^{NEO}, MAL^{FET} and MAL^{MSC} groups. **d)** Pairwise Fisher exact test showing negative log₁₀ adjusted p-values for the gene set enrichment analysis conducted for TCGA *et al.*, 2015, Cirenajwis *et al.*, 2015 and Tsoi *et al.*, 2018 gene signatures. **e)** Heatmap showing the relative expression levels (row z score) of WNT5A high, TP53 high slow cycling cell associated genes in each normal melanocyte and MAL developmental group. **f)** Pairwise Fisher exact test showing negative log₁₀ adjusted p-values for clinicopathological feature and transcriptional categorization within each SKCM group (SKCM^{ADT}, SKCM^{NEO}, SKCM^{FET}, SKCM^{MSC}). There is little to no difference in the enrichment of pigment level, mutation category, or tissue origin between SKCM groups in Figure 4. **g)** Heatmap showing the relative expression levels (row z-score) of immune infiltration program, immune evasion program and FDA-approved therapeutic targets in SKCM groups.

772
773
774
775
776
777
778
779
780
781
782
783
784
785
786
787
788

789 **SUPPLEMENTARY INFORMATION:**

790

791 **SUPPLEMENTAL DISCUSSION**

792 **Supplemental discussion related to Extended Data Figure 3.**

793 The single cell isolation procedure for adult skin was optimized for CKIT+ interfollicular epidermal
794 melanocytes; thus, we expected exclusion of CKIT negative/low follicular melanocyte stem cells (MSC) (see
795 methods). We therefore assessed the expression of known MSC genes^{15,46,47} in each cluster. The lack of expression
796 for known follicular melanocyte stem cell (MSC) genes in group m1 (Extended Data Fig. 3g) suggests the strategy
797 was successful in the adult skin. While, it is possible that CKIT+ differentiated follicular melanocytes were captured,
798 they were not transcriptionally distinct from epidermal melanocytes. In contrast, two of the top 5 ranked genes for
799 group m4, TC4F⁴⁸ and CXCL14⁴⁹ are associated with stem- and progenitor- cell function, suggesting MSCs were
800 captured from fetal hair-bearing, non-volar cutaneous skin (Fig. 1e and Supplemental Table 1, leg and arm).
801 Consistent with this hypothesis, the putative MSC group expressed many of the known MSC genes unlike the other
802 fetal, neonatal and adult clusters (Extended Data Fig. 3g).

803
804 **Supplemental discussion related to Extended Data Figure 6.**

805 Melanocyte development has primarily been studied using non-human model organisms³ or employing *in*
806 *vitro* differentiation of human pluripotent stem cells¹⁹. Gene signatures that define stages of melanocyte
807 differentiation have been identified in these systems, including mouse CD34+ follicular melanocyte stem cells and
808 melanoblasts^{15,16} and *in vitro* human embryonic stem cells, neural crest cells, melanoblasts, and differentiated
809 melanocytes⁵⁰. “Melanoblast” is a designation used to describe committed immature melanocytes along a broad
810 range of developmental time points - from initial commitment to melanocyte fate, which occurs prior to epidermal
811 infiltration through hair follicle morphogenesis, and along two distinct lineage specification pathways³. Given the
812 fetal ages sampled here, we expected observation of *in vivo* human melanoblasts (Extended Data Fig. 7a). If the
813 transcriptional programs of developing melanocytes were conserved from the model systems to *in vivo* human
814 development, we would have expected substantial enrichment for the model system gene sets in the corresponding
815 developmental stage. It was therefore surprising that the published mouse CD34+ melanocyte stem cell signature
816 was the only signature to have relatively high and unique expression within the corresponding human
817 developmental stage profiled here. The observed discordance could have several sources: species-, condition-, or
818 isolation method- specific differences, differences between scRNAseq and bulk mRNAseq, differences in timescale
819 of skin development between species, and/or the type of analysis used to generate the final gene signature.

820 Both the Sennet *et al.* E14.5 melanoblast signature (Extended Data Fig.7b) and the Rezza *et al.* P4 & P5
821 melanocyte signatures (Extended Data Fig.7d) were more highly expressed in the FET, NEO and ADT melanocytes
822 compared to MSCs. In these studies, melanocytic cells were isolated using LEF1 and CKIT expression, and the gene
823 signatures were derived from the comparison of melanocytic cells to other skin cells. In mice, LEF1 is a marker of
824 differentiated (and differentiating) melanocytes and is not expressed in MSCs^{51,52}. Thus, the resulting gene
825 signatures represent a general melanocytic cell-type specific program, exclusive of MSCs, at each mouse
826 developmental time point. The observed low program expression in the human MSC group defined in the current
827 study is therefore consistent with the experimental design for the Sennet and Rezza studies (Extended Data
828 Fig.7b,d). In contrast, the Marie *et al.* melanoblast signature (Extended Data Fig.7c) was derived from the
829 comparison of DCT+ melanoblasts at E15.5 & E17.5 to P1 & P7 melanocytes, and is therefore a melanoblast specific
830 signature. DCT is expressed in differentiated (and differentiating) melanocytes as well as MSCs. Unlike the Sennet
831 *et al.* melanoblast signature, the Marie *et al.* melanoblast signature had decreased expression within more
832 differentiated developmental ages, which is to be expected (Extended Data Fig. 7c). Interestingly, the MSC group
833 had the highest expression. Mouse hair follicle morphogenesis occurs around E14 and is completed postnatally by
834 P8 as a fully mature hair-bearing follicle in anagen phase⁴⁵. In humans, hair follicle formation is reported to start
835 around 10 f.w. with mature hair follicles appearing around 20 f.w. depending on anatomic location and study^{43,44}.
836 The fetal skin specimens in our dataset coincide with the onset and later stages of human hair follicle development,
837 which would encompass morphological stages that resemble mouse hair follicle development at E15.5 and E17.5
838 from Marie *et al.* Unlike mice, human hair-bearing skin contains both hair follicle-associated and epidermal-
839 associated melanocytes. Therefore it is reasonable that the mouse melanoblast-specific program from Marie *et al.*
840 is most highly expressed in a subset of the human fetal melanocytes that express known follicular-associated gene
841 signatures (Extended Data Fig.3g and 7c,e).

842 The *in vitro* derived mature melanocyte gene set was most highly expressed in all groups, with enrichment
843 among FET, NEO, and ADT melanocytes (Extended Data Fig7f). These observations suggest that *in vitro* generation
844 of melanocytes from pluripotent stem cells does not distinguish between differentiating, young and aged
845 melanocytes. Differentiation protocols that better distinguish the *in vivo* profiles reported here, especially
846 accounting for the effect of the aged adult developmental state, would be a valuable tool for the field.
847

848 **Supplemental Discussion Related to Extended Data Fig. 8**

849 A number of studies have identified transcriptional programs associated with a variety of melanoma
850 phenotypes and patient outcomes. Here, we identified four malignant melanoma states identified through
851 classification by the most similar human developmental stage (the MAL groups: MAL^{MSC}, MAL^{FET}, MAL^{NEO}, MAL^{ADT}).
852 We were interested in determining whether any of the MAL group signatures overlapped with, or were enriched
853 for, previously published transcriptional signatures. Two well established transcriptional signatures have been
854 defined as “proliferative / MITF high ” and “invasive / AXL high”^{26,53}. These classifications center on the average
855 expression level of a MITF regulated transcriptional program (inclusive of MITF itself). Since increasing expression
856 of the MITF program is thought to drive a progressively differentiated state⁵⁴, we reasoned the MAL groups, derived
857 from developmental signatures, might likewise present differential expression of the this program. In agreement
858 with this model, the proportion of cells expressing the proliferative and MITF high programs also increased with
859 more differentiated groups (MAL^{ADT} and MAL^{NEO}) as compared to the less differentiated groups (Extended Data Fig.
860 8b-c). In particular, the MAL^{MSC} group comprised almost entirely of invasive melanoma cells and was devoid of MITF
861 high cells, consistent with a dedifferentiated state (Extended Data Fig. 8b-c). Corroborating this interpretation,
862 MAL^{MSC} cells were enriched for TCGA MITF-low signature genes and expressed higher levels of a gene signature
863 indicative of a slow cycling cell therapeutic resistance state associated with stem cells (Extended Data Fig. 8d,e).
864 Thus, we conclude that the stem-like melanoma cells identified here (MAL^{MSC}) are akin to stem-like melanoma cells
865 identified in previous studies. Interestingly, only 1 of the 14 tumors analyzed here was a treatment-naïve tumor
866 (81) but it too contained a small MAL^{MSC} population (approximately 11% of tumor cells), consistent with previous
867 reports describing the presence of a stem-like dedifferentiation state prior to therapy (Extended Data Fig. 8a). We
868 further demonstrate that this program is also expressed in healthy melanocytes (the MSC cells), including
869 enrichment for the slow cycling cell state (Extended Data Fig. 8e) implicating the transcriptional program associated
870 with therapy-resistant, stress-induced, slow cycling tumor cells as a pre-existing feature of MSCs from normal skin
871 as opposed to a feature solely acquired during tumorigenesis or therapeutic exposure.

872 Previous reports have used transcriptional signatures to classify cohorts of melanomas. Most notably, the
873 TCGA cohort⁵⁵ can be classified as “immune”, “keratin”, or “MITF-low”; and the Cirenajwis *et al.* cohort⁵⁶ as
874 “Immune”, “Normal-like”, “Pigmented” or “Proliferative”. Based upon profiling of *in vitro* differentiation of human
875 stem cells into melanocytes, signatures for “undifferentiated”, “neural crest like”, “transition”, and “melanocytic”
876 have also been reported²⁰. We reasoned that the four malignant melanoma states identified here might correspond
877 to the three or four classification signatures reported in these aforementioned studies. As described above, we
878 observed significant enrichment between the MAL^{MSC} group and the TCGA MITF-low signature (Extended Data Fig.
879 8d). We also observed significant enrichment between the MAL^{ADT} group and the Cirenajwis *et al.* “normal-like”
880 signature, consistent with these cells retaining a substantial component of the differentiated melanocyte program.
881 Surprisingly, neither the MAL^{FET} nor the MAL^{NEO} group segregated with previously defined signatures. The MAL^{FET}
882 group was significantly enriched for both the TCGA immune and MITF-low signatures, whereas the MAL^{NEO} group
883 was not enriched for any previously defined signature. These observations suggest that categorization of malignant
884 melanoma cells by the human developmental stage categories defined here represents a novel classification
885 system, with the MAL^{MSC} and MAL^{ADT} groups reasonably aligned with previously reported MITF-low/stem cell and
886 normal melanocytes, respectively, and the MAL^{FET} and MAL^{NEO} groups representing previously unreported
887 signatures. While there was no significant enrichment for the *in vitro* differentiation based gene signatures from
888 Tsoi *et al.* in any of the MAL groups, our analyses suggests that sequential dedifferentiation, which recapitulates
889 the ordered cascade of differentiation in reverse, is predominant in melanoma progression (Extended Data Fig. 8a).
890 This discovery mirrors the findings of Tsoi *et al.* which show that development of therapeutic resistance in
891 melanoma traverses a sequential dedifferentiation trajectory¹⁹.

892
893
894

895 **SUPPLEMENTARY DATA**

896 **Supplementary Table 1:** Related to Fig1 and Fig 2. Donor demographics and cell counts for skin samples used for
897 single cell RNAseq.

898
899 **Supplementary Table 2:** Related to Fig. 2. Differentially expressed genes between donor-matched volar and non-
900 volar cutaneous melanocytes.

901
902 **Supplementary Table 3:** Related to Extended Data Fig. 5. Pairwise differentially expressed genes between
903 melanocyte developmental stages.

904
905 **Supplementary Table 4:** DevMel profile genes from Fig. 3.

906
907 **Supplementary Table 5:** Melanoma dedifferentiation analysis gene set from Fig. 3

908
909 **Supplementary Table 6:** SKCM group categorization of TCGA tumors in Fig. 4 and list of immune and FDA drug
910 targets in Extended Data Fig. 8

911

912

913

914 **METHODS:**

915 **Human Subject details**

916 All skin was collected from surgical discards with informed consent and approval from the UCSF Institutional
917 Review Board. All ages, races/ethnicities, and sexes were included in the eligibility criteria for this study. Adult tissue
918 was obtained from surgical remnants of healthy skin taken for reconstructive surgery or from amputations with
919 healthy skin. Neonatal foreskins were obtained after routine circumcision. Anonymous fetal specimens were
920 obtained from elective terminations and fetal age (stated as fetal weeks) was estimated by heel-toe length³⁷. When
921 possible, fetal sex was determined by visual inspection using a dissecting microscope. All samples were collected in
922 cold CO2 Independent Media (Gibco–Thermo Fisher Scientific) or Medium 154 (Gibco) with 1× Antibiotic-
923 Antimycotic (Gibco) at 4°C until dissociation.

924

925 **Skin sample preparation**

926 Tissue dissociation was started the same day as sample acquisition. For adult and neonatal skin, the
927 epidermis was enzymatically dissociated from the dermis with a dispase, neutral protease, grade II (Roche–Sigma-
928 Aldrich), incubation for 14 hours at 4°C. Epidermal sheets were manually separated from the dermis, finely minced,
929 and incubated with 0.5% trypsin (Gibco) for 3 minutes at 37°C. After manual trituration, trypsin was deactivated
930 using ice cold soybean trypsin inhibitor (Gibco), then diluted 2:3 in ice cold Hanks' balanced salt solution, no Mg²⁺,
931 no Ca²⁺ (Gibco). The dissociated cell suspension was centrifuged at 500g, 4°C, for 4 minutes, resuspended in FACS
932 buffer (0.1% bovine serum albumin (Sigma) and 25mM Hepes (Gibco) in Dulbecco's phosphate-buffered saline
933 (DPBS) (Gibco)) and strained with a 70µM filter to achieve a single cell suspension. For fetal tissue, the developing
934 epidermis was manually removed from the dermis following a 20 – 30 minute incubation with 10mM EDTA
935 (Invitrogen), DPBS at 37°C. The resulting epidermal layer was incubated with 0.5% trypsin (Gibco) for 1 min at 37°C
936 and manually triturated. Trypsin was deactivated using ice cold soybean trypsin inhibitor (Gibco), then diluted 2:3
937 in ice cold Hanks' balanced salt solution (Gibco). The dissociated cell suspension was centrifuged at 500g, 4°C, for 4
938 minutes, resuspended in FACS buffer, and strained with a 70µM filter to achieve a single cell suspension.

939

940 **FACS analysis and single cell sorting**

941 Single cell suspensions were counted, diluted to 1x10⁶ cells/100ul with ice cold FACS buffer containing dye
942 conjugated antibodies (anti-CKIT (104D2), 15ng/100µl (CD11705, Thermo Fisher Scientific), anti-ITGA6 (GoH3),
943 15ng/100µl (12-0495-82, Thermo Fisher Scientific) and CD11c, 1:20 dilution (46-0116-41, Thermo Fisher Scientific))
944 and incubated on ice for 25 minutes. Cells were washed one time with 10x volume of FACS buffer, centrifuged for
945 2 minutes at 500g, resuspended in 30ng/mL Dapi (D3571, Molecular Probes), FACS buffer. Resuspended cells were
946 strained through a 35 µm nylon mesh filter and kept on ice until sorted.

947 Single cells were sorted into 384-well plates using the “Ultra purity” setting on a SH800S (Sony) sorter. For
948 a typical sort, a tube containing 0.3-1ml the pre-stained cell suspension was vortexed gently and loaded onto the
949 FACS machine. A small number of cells were flowed at low pressure to check cell concentration and amount of
950 debris. Then the pressure was adjusted, flow was paused, the first destination plate was unsealed and
951 loaded. Single cells were sorted into plates by gating to exclude dead/dying cells (DAPI+) and doublets. The majority
952 of the plate contained melanocytes (CD11c-/CKIT+) with 4 to 5 columns of basal keratinocytes (CD11c-/CKIT-
953 /ITGA6+) and other triple negative cells such as suprabasal keratinocytes (CD11c-/CKIT-/ITGA6-). Immediately, after
954 sorting, plates were sealed with a pre-labeled aluminum seal, centrifuged at 4°C and flash frozen on dry ice, before
955 storage at -80 for later use.

956

957 **Lysis plate preparation**

958 Lysis plates were created by dispensing 0.4 µl lysis buffer (0.5U Recombinant RNase Inhibitor (Takara Bio,
959 2313B), 0.0625% Triton™ X-100 (Sigma, 93443-100ML), 3.125 mM dNTP mix (Thermo Fisher, R0193), 3.125 µM
960 Oligo-dT30VN (IDT, 5’AAGCAGTGGTATCAACGCAGAGTACT30VN-3’) and 1:600,000 ERCC RNA spike-in mix (Thermo
961 Fisher, 4456740)) into 384-well hard-shell PCR plates (Biorad HSP3901) using a Tempest liquid handler (Formulatrix).
962 All plates were then spun down for 1 minute at 3220xg and snap frozen on dry ice. Plates were stored at -80°C until
963 used for sorting.

964

965 **cDNA synthesis and library preparation**

966 cDNA synthesis was performed using the Smart-seq2 protocol (Picelli et al., 2013, 2014). Briefly, 384-well
967 plates containing single-cell lysates were thawed on ice followed by first strand synthesis. 0.6 µl of reaction mix
968 (16.7 U/µl SMARTScribe Reverse Transcriptase (Takara Bio, 639538), 1.67 U/µl Recombinant RNase Inhibitor (Takara
969 Bio, 2313B), 1.67X First-Strand Buffer (Takara Bio, 639538), 1.67 µM TSO (Exiqon, 5’-
970 AAGCAGTGGTATCAACGCAGACTACATrGrG+G-3’), 8.33 mM DTT (Bioworld, 40420001-1), 1.67 M Betaine (Sigma,
971 B0300-5VL), and 10 mM MgCl₂ (Sigma, M1028-10X1ML)) was added to each well using a Tempest liquid handler or
972 Mosquito (TTP Labtech). Reverse transcription was carried out by incubating wells on a ProFlex 2x384 thermal-
973 cycler (Thermo Fisher) at 42°C for 90 min and stopped by heating at 70°C for 5 min. Subsequently, 1.5 µl of PCR mix
974 (1.67X KAPA HiFi HotStart ReadyMix (Kapa Biosystems, KK2602), 0.17 µM IS PCR primer (IDT, 5’-
975 AAGCAGTGGTATCAACGCAGAGT-3’), and 0.038 U/µl Lambda Exonuclease (NEB, M0262L)) was added to each well
976 with a Mantis liquid handler (Formulatrix) or Mosquito, and second strand synthesis was performed on a ProFlex
977 2x384 thermal-cycler by using the following program: 1. 37°C for 30 minutes, 2. 95°C for 3 minutes, 3. 23 cycles of
978 98°C for 20 seconds, 67°C for 15 seconds, and 72°C for 4 minutes, and 4. 72°C for 5 minutes. The amplified product
979 was diluted with a ratio of 1 part cDNA to 10 parts 10mM Tris-HCl (Thermo Fisher, 15568025). 0.6 µl of diluted
980 product was transferred to a new 384-well plate using the Viaflow 384 channel pipette (Integra). Illumina
981 sequencing libraries were prepared as described in (Darmanis et al., 2015). Briefly, tagmentation was carried out
982 on double-stranded cDNA using the Nextera XT Library Sample Preparation kit (Illumina, FC-131-1096). Each well
983 was mixed with 0.8 µl Nextera tagmentation DNA buffer (Illumina) and 0.4 µl Tn5 enzyme (Illumina), then incubated
984 at 55°C for 10 min. The reaction was stopped by adding 0.4 µl “Neutralize Tagment Buffer” (Illumina) and spinning
985 at room temperature in a centrifuge at 3220xg for 5 min. Indexing PCR reactions were performed by adding 0.4 µl
986 of 5 µM i5 indexing primer, 0.4 µl of 5 µM i7 indexing primer, and 1.2 µl of Nextera NPM mix (Illumina). All reagents
987 were dispensed with the Mantis or Mosquito liquid handlers. PCR amplification was carried out on a ProFlex 2x384
988 thermal cycler using the following program: 1. 72°C for 3 minutes, 2. 95°C for 30 seconds, 3. 12 cycles of 95°C for
989 10 seconds, 55°C for 30 seconds, and 72°C for 1 minute, and 4. 72°C for 5 minutes. Library pooling, quality control,
990 and sequencing. Following library preparation, wells of each library plate were pooled using a Mosquito liquid
991 handler. Pooling was followed by two purifications using 0.7x AMPure beads (Fisher, A63881). Library quality was
992 assessed using capillary electrophoresis on a Fragment Analyzer (Agilent) or TapeStation (Agilent), and libraries were
993 quantified by qPCR (Kapa Biosystems, KK4923) on a CFX96 Touch Real-Time PCR Detection System (Biorad). Plate
994 pools were normalized to 2 nM and equal volumes from library plates were mixed together to make the sequencing
995 sample pool.

996

997 **Sequencing libraries from 384-well plates**

998 Libraries were sequenced on the NextSeq or NovaSeq 6000 Sequencing System (Illumina) using 2 x 100bp
999 paired-end reads and 2 x 8bp or 2 x 12bp index reads. NextSeq runs used high output kits, whereas NovaSeq runs
1000 used either a 200 or 300-cycle kit (Illumina, 20012860). PhiX control library was spiked in at 1%.

1001 1002 **Single-cell transcriptomic processing and analysis**

1003 Single cell reads were mapped to the human reference hg38 containing ERCC sequences using STAR
1004 aligner³⁸. HTSeq³⁹ was used to create gene count tables. These count tables were compiled and processed using
1005 Scanpy⁴⁰. Low-quality cells were filtered based on the following criteria: number of genes < 1,250 OR number of
1006 reads < 50,000. Each gene in the transcriptome exhibited read counts in at least 3 cells. Cells exhibiting > 2-fold
1007 higher number of genes than average were labeled as putative doublets and removed. Iterative Louvain clustering
1008 yielded cell type-specific clusters, which were annotated using published marker genes based on inter-cluster
1009 differential expression analysis (two-sided Mann Whitney U test, Benjamini-Hochberg FDR < 5%). Briefly, Louvain
1010 clustering was performed on the k-nearest neighbor graph in principle component space of scaled highly variable
1011 genes. Cells were visualized using 2-dimensional UMAP embeddings. Cell cycle status was inferred by the mean
1012 ranked expression of marker genes, referred to as the cell cycle program score⁴¹. Cells below the 95th-percentile of
1013 the cell cycle program score were labeled non-cycling; conversely, cells equal to or greater than 95th-percentile of
1014 the cell cycle program score were labeled cycling. In order to control for variance introduced by disproportionate
1015 populations of cycling cells across groups, non-cycling cells were considered for downstream analyses. Thus,
1016 anatomical site-specific analyses and human melanocyte differentiation programs analyses were conducted on non-
1017 cycling cells.

1018 1019 **Percent v-mel and c-mel**

1020 Top-10 cutaneous and top-10 volar DEGs were identified from the site-enriched genes based on highest
1021 median per-patient log-fold-change between cutaneous and volar samples. Individual cells were classified as v-mel
1022 if 4 or more top-10 volar DEGs exhibited non-zero expression AND fewer than 4 top-10 cutaneous DEGs exhibited
1023 non-zero expression. Conversely, individual cells were classified as c-mel if 4 or more top-10 cutaneous DEGs
1024 exhibited non-zero expression AND fewer than 4 top-10 volar DEGs exhibited non-zero expression. Percent v-mel
1025 and c-mel were then calculated for each skin specimen of unique anatomical location from each individual patient.

1026 To determine the percent of HPGD positive melanocytes in tissue sections, melanocytes (TYRP1+ cells)
1027 were manually counted. Fraction of cells was determined by the number of HPGD+ TYRP1+ cells divided by the
1028 total number of TYRP1+ cells from each fixed frozen section. To quantify the number of NTRK2 and HPGD foci per
1029 DCT+ cells from the RNAscope data, images were processed to correct for Opal 570 (HPGD) bleed-through into the
1030 Opal 620 (NTRK2) channel. After bleed-through correction, DCT and associated dapi signal was used to define the
1031 area of DCT+ cells. NTRK2 and HPGD foci within DCT+ cells were then manually counted manually. All Image analysis
1032 was performed in Fiji (<http://fiji.sc/>)

1033 1034 **Immunofluorescence**

1035 Skin samples were fixed in 4% paraformaldehyde (Electron Microscopy Sciences) at 4 °C overnight, washed
1036 with cold DPBS prior to paraffin or OCT embedding. Fixed frozen skin sections were incubated in blocking buffer:
1037 2.5% donkey serum, 2.5% goat serum (Jackson ImmunoResearch Laboratories), 1% bovine serum albumin (Sigma-
1038 Aldrich), and 0.1% Triton X-100 (Sigma-Aldrich) for 1–2 hours at room temperature. The following primary
1039 antibodies were used at the indicated concentration in blocking buffer overnight at 4°C: mouse monoclonal anti-
1040 TYRP1 1:200 (TA99, ab3312, Abcam), mouse monoclonal anti-CKIT 1:100 (CD11700, Invitrogen–Thermo Fisher
1041 Scientific), rabbit polyclonal anti-HPGD 1:100 (HPA005679, Sigma-Aldrich). Secondary antibodies against mouse IgG,
1042 or rabbit IgG conjugated to DyLight 488 or 594 (Thermo Fisher Scientific) were used at a 1:1,000 dilution for 1–2 h
1043 at room temperature followed by Dapi, 1:1000 (Molecular Probes) for 1 minute. Sections were mounted in
1044 VECTASHIELD Vibrance (Vector Laboratories) prior to imaging.

1045 Immunofluorescence images were acquired using Nikon NIS-Elements multi-platform acquisition software
1046 on an fully automated Nikon Ti-E inverted microscope with an Apo TIRF, 60x, 1.49 NA, oil objective (Nikon) and a
1047 Clara CCD camera (Andor).

1048 1049 **Multiplex RNA-FISH**

We performed Multiplex RNA-FISH using the RNAscope Assay RNAscope Multiplex Fluorescent V2 assay (Bio-technie, Cat. No. 323110) kit according to manufacturer's protocol on 10 μ M FFPE tissue sections. Tissues were stained using probes purchased from ACD for *HPGD* (Channel 1), *NTRK2* (Channel 2), *DCT* (Channel 3) and TSA Opal 570 (Channel 1, Akoya Biosciences, Cat. No. FP1488001KT), TSA Opal 620 (Channel 2, Akoya Biosciences, Cat. No. FP1488001KT) and TSA Opal 690 (Channel 3, Akoya Biosciences, Cat. No. FP1497001KT). TSA was used at a 1:1500 dilution. Cells were counterstained with DAPI and mounted with Prolong Gold Antifade Mountant (Thermo Fisher, P36930). Tissues were imaged using an Leica DMI8 microscope.

Diffusion Pseudotime

Diffusion pseudotime analysis on all non-cycling melanocyte cells was performed using the `scanpy.tl.dpt` function. The pseudotime reference root cell was chosen from the youngest sample (9.5 f.w.). The diffusion map was computed from an $n=30$ neighborhood graph with a Gaussian kernel.

Single cell developmental stage melanocyte (DevMel) logistic regression model

Input data was composed of single cell transcriptomes from the following 4 groups: MSC, FET, NEO and ADT. The input examples were randomly sampled and the number of examples was balanced among all labels. The combination of normal and melanoma transcriptomes was used to scale and center the data. The input data was split into testing and training partitions at a ratio 33:67. We implemented elasticnet regularization with an $l1$ ratio = 0.8. Single cell transcriptomes were evaluated by the model to yield a developmental stage label.

Classification of genes in melanoma dedifferentiation categories

Logistic regression variables and top-100 differentially expressed genes for each melanoma cell population grouped by DevMel label were used in subsequent dedifferentiation pathway analysis. DevMel group mean ranked expression was compared between normal and melanoma datasets to determine pathway based on the following criteria:

Direct dedifferentiation: All cancer DevMel group \geq mean normal non-ADT DevMel group, 4-fold normal ADT DevMel group $<$ mean normal non-ADT DevMel group

Sequential dedifferentiation: Max cancer DevMel group $=$ Max normal DevMel group

Melanoma-specific: For each, cancer DevMel group $>$ corresponding normal DevMel group, All cancer DevMel groups $>$ 40th-percentile of expression, All normal DevMel groups $<$ 10th-percentile of expression

Normal-specific: For each, cancer DevMel group $<$ corresponding normal DevMel group, All cancer DevMel groups $<$ 10th-percentile of expression, All normal DevMel groups $>$ 15th-percentile of expression

Down regulated: All cancer DevMel group \leq mean normal non-ADT DevMel group, Normal ADT DevMel group $>$ 1.5-fold mean normal non-ADT DevMel group

Not-readopted: All cancer DevMel group \leq normal ADT DevMel group, 1.5-fold normal ADT DevMel group $<$ mean normal non-ADT DevMel group

Bulk tumor deconvolution

CIBERSORT²⁹ was used to deconvolve bulk RNA-seq from the SKCM-TCGA cohort. As input, CIBERSORT requires cell type-labeled transcriptomes to estimate the proportion of each cell type in a bulk RNA-seq sample. Here, trimmed both single cell and bulk RNA-seq transcriptomes to include only genes that are shared in both datasets. Adopting a k-fold cross-validation approach, we prepared 10 sets of single cell input transcriptomes from normal melanocytes across 4 developmental stages: MSC, FET, NEO and ADT (balanced cell counts across all labels). Each input transcriptome set was used to devolve the SKCM-TCGA bulk RNA-seq samples, yielding 10 estimates of cell proportion. For each individual sample in the SKCM-TCGA dataset, the label means were used as the final estimate of label proportion. Hierarchical clustering was used to group SKCM-TCGA samples based on similar label proportions. One-sided Fisher Exact test was used to determine significant enrichment between two gene lists. The lifelines python package (10.5281/zenodo.3833188) was used to create Kaplan-Meier survival plots and perform logrank tests using curated SKCM-TCGA metadata⁴².

Data availability

Jupyter notebooks with detailed analysis scripts are available at: github.com/czbiohub/human_melanocytes

L103 GEO: GSE151091
L104 Bioproject: PRJNA625154
L105 SAMN14593853 : A1015LM
L106 SAMN14593854 : 12WKM01
L107 SAMN14593855 : FS043_LM
L108 SAMN14593856 : A1011L
L109 SAMN14593857 : A1020LM
L110 SAMN14593858 : A1033M
L111 SAMN14593859 : A1022M
L112 SAMN14593860 : A1014L
L113 SAMN14593861 : A1038LM
L114 SAMN14593862 : A1026L
L115 SAMN14593863 : A1021M
L116 SAMN14593864 : FS030_LM
L117 SAMN14593865 : A1016LM
L118 SAMN14593866 : A1025L
L119 SAMN14593867 : A1017LM
L120 SAMN14593868 : A1012M
L121 SAMN14593869 : 18WKM06
L122 SAMN14593870 : 12WK05
L123 SAMN14593871 : 10WK03
L124 SAMN14593872 : 16WKM04
L125 SAMN14593873 : 9.5WK02
L126 SAMN14593874 : A1046M
L127